energies

MDPI

Article

Novel Ni/Ce(Ti)ZrO_2 Catalysts for Methane Dry Reforming Prepared in Supercritical Alcohol Media

Yuliya Bespalko [1,*], Ekaterina Smal [1,2], Mikhail Simonov [1,2], Konstantin Valeev [1], Valeria Fedorova [1], Tamara Krieger [1,2], Svetlana Cherepanova [1,2], Arcady Ishchenko [1,2], Vladimir Rogov [1,2] and Vladislav Sadykov [1,2]

[1] Department of Heterogeneous Catalysis, Boreskov Institute of Catalysis, 630090 Novosibirsk, Russia; alageizia@mail.ru (E.S.); smike@catalysis.ru (M.S.); valeev@catalysis.ru (K.V.); valeria@catalysis.ru (V.F.); krieger@catalysis.ru (T.K.); svch@catalysis.ru (S.C.); arcady.ishchenko@gmail.com (A.I.); rogov@catalysis.ru (V.R.); sadykov@catalysis.ru (V.S.)

[2] Department of Natural Sciences, Novosibirsk State University, 630090 Novosibirsk, Russia

* Correspondence: bespalko@catalysis.ru; Tel.: +7-383-3269-511

Received: 20 May 2020; Accepted: 26 June 2020; Published: 1 July 2020

Abstract: To achieve a high activity and coking stability of nickel catalysts in dry reforming of methane, materials comprised of ceria–zirconia doped by Ti were investigated as supports. Ceria–zirconia supports doped with titanium were prepared either via the Pechini method or by synthesis in supercritical alcohol media. Ni-containing catalysts were prepared by two techniques: standard incipient wetness impregnation and one-pot synthesis. The catalytic reaction of DRM to synthesis gas was carried out in the 600–750 °C range over 5% wt. Ni/Ce(Ti)ZrO_2. Dried and calcined supports and catalysts were characterized by physicochemical methods including N_2 adsorption, XRD, Raman, H_2-TPR, and HRTEM. Both preparation methods led to formation of solid solution with cubic fluorite-like structure, as well as after addition of Ti. Introduction of Ti should provide improved oxygen storage capacity and mobility of support oxygen. The highest activity was observed with the catalyst of 5% wt. Ni/$Ce_{0.75}Ti_{0.2}Zr_{0.05}O_{2-\delta}$ composition due to optimized oxide support structure and support oxygen mobility.

Keywords: ceria–zirconia; supercritical synthesis; dry reforming of methane; biogas

1. Introduction

Dry reforming of methane (DRM) is reaction ($CH_4 + CO_2 = 2H_2 + 2CO$) for biogas utilization into two useful resource gases—Hydrogen and carbon monoxide. The obtained syngas is characterized by a ratio of $H_2/CO \leq 1$, which makes it suitable for oxygenate synthesis [1–3].

Over the last several years, a large number of studies have been focused on the Ni-based DRM catalysts, which proved to be very promising for the practical application due to their high activity and low cost [1,4–10]. However, the main problem of these catalysts is the rapid deactivation caused by nickel sintering and coke formation. Many research studies aimed to increase catalytic activity and stability by controlling the morphology of the active component and using it in the form of highly dispersed nano-particles, which should minimize carbon formation [11,12]. Since the process of coking is sensitive to the support structure and dispersion of active metal deposited on the catalyst surface is very important, activity and stability of catalysts can be provided by developing supports with required characteristics. Fibrous carbon deposition occurs on relatively large active metal particles. Agglomeration of metal clusters and coking can be prevented using supports with a strong metal-support interaction as well as a high reactivity and mobility of the surface/lattice oxygen. Ceria has been extensively studied in the literature, and the oxygen storage capacity of ceria can be increased

by doping with various cations [6,13–16]. Doping of ceria by zirconium cations resulted in formation of ceria–zirconia solid solutions in all ranges of compositions and led to improved textural and catalytic properties, thermal resistance, and oxygen transport properties [17]. In [18], authors investigated $Ce_{0.75}Zr_{0.25}O_2$ and confirmed that Zr doping induces a severe distortion of the atomic structures, and formation of oxygen vacancies around the doping Zr promotes reduction of two neighboring Ce cations by the electrons left by the eliminated oxygen atom. According to [13,19], the formation of a pair "interstitial oxygen-anion vacancy" and additional Ce^{3+} anions occurs. $Ce_{1-x}Zr_xO_2$ solid solutions are promising supports for Ni-based catalysts due to their thermal stability and resistance to coke formation because of the high reactivity and mobility of the surface/lattice oxygen, as well as their ability to accumulate oxygen due to easy redox process of Ce^{4+}/Ce^{3+} [20,21]. The substitution of up to 20% of cerium by doping cations (zirconium) leads to the formation of solid solutions with a cubic structure, that in turn increases the ability of Ce^{4+} cations to be reduced and improves the thermal stability of catalysts [18]. The coke formation in DMR was not directly associated with the activity, but apparently depended on the Ce/Zr ratio. A basic ratio of [Ce]/[Zr] = 3/1 was chosen since it was proved to provide the best catalyst stability in reforming of methane [22].

In the case of triple oxide support, doping cations can be aliovalent or isovalent—With different or identical charges, respectively. Thus, doping of $Ce_{0.75}Zr_{0.25}O_2$ oxide with 2+ and 3+ charged cations reduces the temperature at which redox processes take place. This can be explained by enhanced diffusion of lattice oxygen due to formation of vacancies in the anion sublattice. Moreover, incorporation of isovalent cations improves such textural properties as the surface area and stability to sintering. Among the catalysts tested, samples with composition of 5 wt% $Ni/Ce_{0.5}Zr_{0.33}M_{0.17}O_{2-\delta}$ (M = Ca, La, and Y) show the highest activity for DMR along with improved functional characteristics such as oxygen storage capacity, pore volume/surface area, reducibility, good nickel dispersion, and surface nickel content [23].

Incorporation of doping cations like Ti with ionic radius smaller than Ce leads to change of bonds length in the oxygen lattice and to increased oxygen mobility [24]. A series of $Ce_xTi_{1-x}O_2$ mixed oxides with cubic phase was synthesized [25]. Ti^{4+} ions substituted for Ce^{4+} ions forming solid solution of $Ce_xTi_{1-x}O_2$. Both cerium (4+) and titanium (4+) cations can change their charge to 3+, so reducibility of the solid solution or oxygen storage capacity should be higher compared to cerium oxide or titanium oxide [24,25]. For $Ce_{0.7}Ti_{0.3}O_2$, the superior activity is attributed to the enhanced redox properties together with the modification of surface acid–base sites, provided by the proper formation of Ce–O–Ti linkage bonds [26].

Synthesis and preparation process affect different properties of Ce-based materials such as phase composition, particle size, and textural characteristics. Mixed CeO_2-ZrO_2 systems can be prepared using various methods including solid state synthesis [27,28], co-precipitation [16,29–31], sol-gel [31,32], microemulsion [33,34], high energy ball milling [35,36], and hydrothermal and solvothermal synthesis [37,38].

Synthesis in supercritical fluids (SCS) is useful to prepare complex mixed oxides in a high dispersion state and allows for providing high effectiveness, especially in continuous mode [39–42]. Continuous synthesis in supercritical media is a method to prepare metal oxide nanoparticles using supercritical alcohols. Processes of forced hydrolysis, nucleation, and growth of the oxide nanoparticles occurred under supercritical conditions. When using the method of supercritical synthesis, alcoholic solutions of metal precursors are mixed with supercritical alcohols under rapid heating, which allows to obtain nanoparticles of metal oxides quickly and continuously. In our previous work, mixed Ce–Zr oxides prepared using ethanol and isopropanol as a supercritical medium in a flow reactor were studied [43,44]. It has been shown that the use of chelating agents such as acetylacetone can prevent selective polymerization of zirconium hydroxo-complexes, stabilize colloidal particles, and, thereby, increase the uniformity of the components' distribution in the complex oxide. Mixed CeO_2-ZrO_2 oxides with different Ce:Zr ratios show such favorable properties as relatively high homogeneity,

thermal stability, and resistance to sintering, acceptable surface area, and porosity, which make them promising supports for DRM catalysts.

An important characteristic of the catalyst preparation is the method of active component introduction: impregnation of supports [7,9,43,45] or one-pot routes [6,7,46–49], which influence Ni interaction with support (dispersion, stability, etc.). The method of synthesis of so called one-pot samples repeats the method of obtaining complex oxides; the main difference is that the solution of the nickel precursor is fed to the reactor simultaneously with the precursors of the oxide carrier.

The aim of this work is to investigate the effect of the partial substitution of Zr^{4+} by Ti^{4+} in $Ce_{0.75}Zr_{0.25}O_2$ support on microstructure, physico-chemical, and catalytic properties of prepared samples in the dry reforming of methane. $Ce_{0.75}(Ti,Zr)_{0.25}O_2$ oxides with different Ti:Zr molar ratios have been prepared by two techniques: polymerized precursors method and solvothermal synthesis in supercritical isopropanol with subsequent nickel supporting by impregnation. For the first time, we have carried out the one-pot synthesis of 5% Ni/Ce(Ti)ZrO_2 oxides using the SCS method, and for comparison, we have also prepared one-pot catalysts using the Pechini method. Advantages of processing in supercritical isopropanol include crystallization of Ce(Ti)ZrO_2 mixed oxides at significantly lower temperatures than by using common synthesis, as well as less time and energy costs; moreover, the microstructure can be tuned at the nanosized level, providing material with a higher surface area and phase purity.

The specificity of catalytic performance of catalysts based on ceria–zirconia supports with different composition prepared by two methods was analyzed, taking into account a spatial homogeneity of complex oxides, morphology, Ni dispersion, and thermal stability. In order to clarify the effect of Ti doping, materials were studied by N_2 adsorption, X-ray diffraction (XRD), Raman spectroscopy, high-angle annular dark field scanning transmission electron microscopy (HAADF-STEM), high-resolution transmission electron microscopy (HRTEM), temperature-programmed reduction by hydrogen (H_2 TPR) and tested in methane dry reforming.

2. Materials and Methods

2.1. Support Preparation

$Ce_{0.75}Zr_{0.25}O_{2-\delta}$ and $Ce_{0.75}Ti_xZr_{0.25-x}O_{2-\delta}$ (x = 0.1, 0.2) oxides were prepared by the solvothermal continuous synthesis using isopropanol along with acetylacetone as a complexing agent, which was added into the Zr solution at a 2:1 molar ratio to Zr amount. $Zr(OBu)_4$ (Alfa Aesar, 80% solution in n-butanol) and $Ce(NO_3)_3{\cdot}6H_2O$ (Vecton, pure for analysis grade), $Ti[O(CH_2)_3CH_3]_4$ (Acros Organics) isopropanol solutions were used as Zr and Ce precursors. The experimental custom-built setup used for preparation of Ce(Ti)ZrO_2 supports and one-pot catalyst series in SC conditions is shown in Figure 1. The mixture of the Ce and Zr precursor solutions was fed into a U-shaped reactor (l = 1 m, inner d = 4 mm) at a rate of 5 mL/min along with isopropanol preheated to 150 °C, which flow rate was 9 mL/min at T = 400 °C and P = 120 atm.

For comparison, $Ce_{0.75}Zr_{0.25}O_{2-\delta}$ sample was synthesized by a modified polymerized precursor (Pechini) route using $Ce(NO_3)_3{\cdot}6H_2O$ (Vecton, pure for analysis grade) and $Zr(OCl)_2$ (Vecton, pure for analysis grade). Ethylene glycol (EG) and citric acid (CA) were used as complexing agents. The reagents were taken in the following molar ratios CA: EG: metal (Ce + Zr) = 3.75:11.25:1. Citric acid in the ratio 1:3 was dissolved in EG; the corresponding salts were added until completely dissolved. The solution was heated and thickened, becoming a dark yellow one. The obtained gel was dried at a temperature of 80 °C for 12 h and calcined in static air by heating at a rate of 5 °C/min from room temperature to 700 °C.

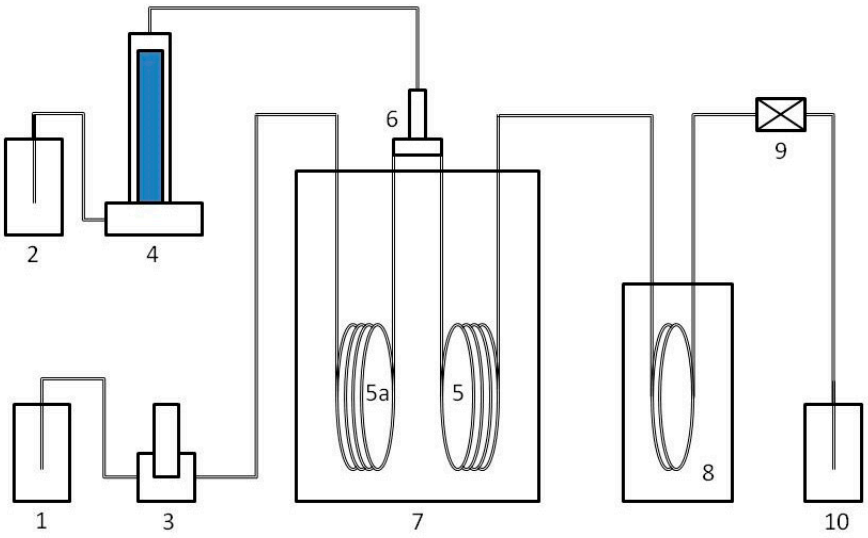

Figure 1. Scheme of the setup with flow reactor for synthesis in supercritical media. (1) Container with alcohol, (2) container with a solution of metal salts, (3) plunger pump, (4) syringe pump, (5) reactor, (5a) alcohol preheating element, (6) mixer, (7) oven, (8) heat exchanger, (9) back pressure valve, and (10) storage container.

2.2. Catalysts Preparation

In the case of obtaining catalysts by both impregnation and one-pot synthesis, the loading amount of Ni was fixed at 5 wt%.

The $Ni/Ce_{0.75}Zr_{0.25}O_{2-\delta}$ and $Ni/Ce_{0.75}Ti_xZr_{0.25-x}O_{2-\delta}$ catalysts were prepared by the incipient wetness impregnation of oxides obtained by both methods (Pechini and SCS) with the necessary amount of $Ni(NO_3)_2{\cdot}6H_2O$.

For one-pot synthesis via the Pechini route, the required amount of $Ni(NO_3)_2{\cdot}6H_2O$ (Vecton, pure for analysis) was added into EG solution containing all other elements (vide supra).

For one-pot synthesis in supercritical conditions, the required quantities of $Ni(NO_3)_2{\cdot}6H_2O$ (Vecton, pure for analysis) and $Ce(NO_3)_3{\cdot}6H_2O$ were combined in isopropanol and mixed with $Zr(OBu)_4$ and $Ti[O(CH_2)_3CH_3]$. The mixed solution was fed into the reactor and SCS was performed under the same conditions as for obtaining carriers. All precursors were dried and calcined at 700 °C for 2 h.

2.3. Characterization

All materials were characterized using a complex of methods. X-ray diffraction analysis was carried out using a D8 Advance (Bruker, Germany) diffractometer with Cu Ka radiation and LynxEye detector. XRD pattern were collected in 2Θ range 20–85 °C with 0.05 step size and 3 s accumulation times. The fraction of oxygen vacancies was counted from refinement of occupancy of oxygen positions in the structure by the Rietveld method using the TOPAS (Total Pattern Analysis System) program (Bruker, Germany). High-angle annular dark field scanning transmission electron microscopy (HAADF-STEM) and high-resolution transmission electron microscopy (HRTEM) images were obtained with a JEM-2200FS transmission electron microscope (JEOL Ltd., Tokyo, Japan, acceleration voltage 200 kV, lattice resolution 1 Å) equipped with a Cs-corrector and an EDX spectrometer (JEOL Ltd., Tokyo, Japan). The minimum spot diameter for the step-by-step line or mapping elemental EDX analysis was ~1 nm with a step of about 1.5 nm. FT-Raman spectra were recorded in the 3600–100 cm^{-1} range with 300 scans using an RFS 100/S Bruker spectrometer. Experimental spectra were gained in the backscattering geometry using the 514.5 nm line of an Ar+ laser. The spectral resolution was 4 cm^{-1} and 180° geometry. The texture of samples was studied by N_2 adsorption isotherms at −196 °C using an ASAP-2400 instrument (Micromeritics, Norcross, GA, USA). Prior to analysis, samples were degassed at 150 °C under vacuum for 16 h. The micropore volume was determined by t-plot analysis.

The mean pore size was evaluated as 4V/A. The specific surface area of materials was estimated with a SORBI N.4.1 apparatus by the four-point BET method. Prior to measurements, samples were pretreated at 200 °C in vacuum for 1 h. Redox properties of supports and catalysts were studied by the temperature programmed reduction by H_2 (H_2-TPR) with the temperature ramp 10°/min from 60–900 °C in the mixture of argon (90%) with hydrogen (10%) content recorded by GC Tsvet 500 (Russia).

2.4. Catalytic Reaction

Methane dry reforming reaction was carried out in a tubular quartz plug flow reactor with catalyst sample diluted with quartz (particle size fraction of 0.5–0.25 mm) in a 1:1 ratio using the feed of 15% CH_4 + 15% CO_2 + N_2 balance at 600–750 °C and contact time 10 ms. Concentrations of initial reagents and products were detected on-line with a Test-201 (Bonair, Russia) gas analyzer. Before reaction, catalysts were pretreated in 10 vol% O_2/N_2 at 600 °C for 30 min, then reduced in 5 vol% H_2/N_2 at 600 °C for one hour. The variation of temperature in the range of 600–750–600 °C was realized stepwise (temperature rise and decline with an interval of 50 °C) for comparison of effects of thermal cycling. Concentrations of reagents at each step were registered during 30 min with contact time 10 ms.

3. Results and Discussion

3.1. Structural Properties of Supports and Ni/$Ce_{0.75}Zr_{0.25}O_{2-\delta}$

Compositions and abbreviations of prepared samples are presented in Table 1.

Table 1. Structural properties of as prepared supports and 5% Ni/Ce(Ti)ZrO_2 catalysts according to XRD.

Code	Method of Synthesis	Composition	Lattice Parameter, Å	Crystallite Size, nm	
			Fluorite Phase	Oxide	NiO
CZ_p	Pechini	$Ce_{0.75}Zr_{0.25}O_{2-\delta}$	5.356 (1)	10.4	-
$Ni/CZ_{P\text{-}im}$	Pechini; impregnated	$Ni/Ce_{0.75}Zr_{0.25}O_{2-\delta}$	5.357 (1)	10.7	18
$Ni/CZ_{P\text{-}op}$	Pechini; «one-pot»	$Ni/Ce_{0.75}Zr_{0.25}O_{2-\delta}$	5.358 (1)	11.7	70
CZ_{sc}	SCS	$Ce_{0.75}Zr_{0.25}O_{2-\delta}$	5.368 (1)	8.8	-
$Ni/CZ_{sc\text{-}im}$	SCS; impregnated	$Ni/Ce_{0.75}Zr_{0.25}O_{2-\delta}$	5.368 (1)	9.4	30
$Ni/CZ_{sc\text{-}op}$	SCS; «one-pot»	$Ni/Ce_{0.75}Zr_{0.25}O_{2-\delta}$	5.371 (1)	8.9	19
$CT_{0.1}Z_{sc}$	SCS;	$Ce_{0.75}Ti_{0.1}Zr_{0.15}O_{2-\delta}$	5.378 (1)	10.0	-
$CT_{0.2}Z_{sc}$	SCS;	$Ce_{0.75}Ti_{0.2}Zr_{0.05}O_{2-\delta}$	5.393 (1)	9.0	-
$Ni/CT_{0.1}Z_{sc\text{-}im}$	SCS; impregnated	$Ni/Ce_{0.75}Ti_{0.1}Zr_{0.15}O_{2-\delta}$	5.379 (1)	10.4	20
$Ni/CT_{0.1}Z_{sc\text{-}op}$	SCS; «one-pot»	$Ni/Ce_{0.75}Ti_{0.1}Zr_{0.15}O_{2-\delta}$	5.376 (1)	8.5	13
$Ni/CT_{0.2}Z_{sc\text{-}op}$	SCS; «one-pot»	$Ni/Ce_{0.75}Ti_{0.2}Zr_{0.05}O_{2-\delta}$	5.393 (1)	8.5	15

As follows from the XRD patterns (Figures 2 and 3), $Ce_{0.75}Zr_{0.25}O_{2-\delta}$ samples prepared by both synthesis methods have the same fluorite crystal structure. However, there is an increase in the lattice constants for the CZsc sample prepared by the supercritical method (5.369 Å) compared to the CZ_P sample (5.356 Å), suggesting a higher disordering of its structure.

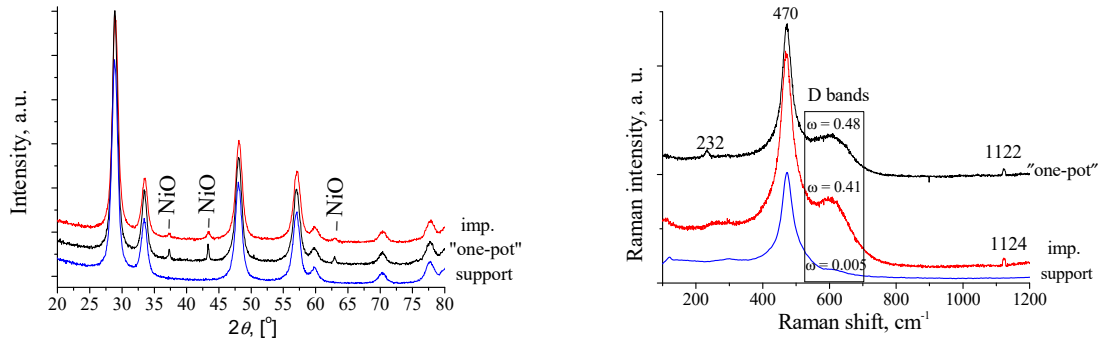

(**a**) (**b**)

Figure 2. XRD patterns (**a**) and Raman spectra (**b**) of $Ni/Ce_{0.75}Zr_{0.25}O_{2-\delta}$ catalysts prepared via the Pechini method and calcined at 700 °C.

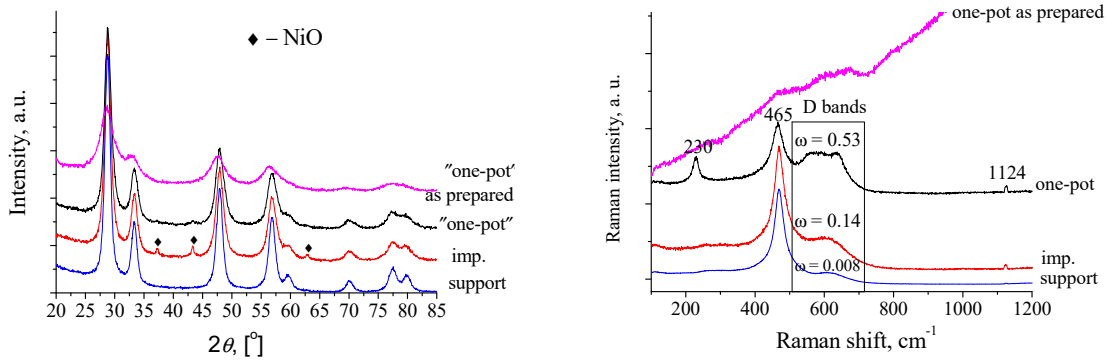

(**a**) (**b**)

Figure 3. XRD patterns (**a**) and Raman spectra (**b**) of $Ni/Ce_{0.75}Zr_{0.25}O_{2-\delta}$ catalysts prepared in supercritical conditions and calcined at 700 °C.

Figure 1a shows the XRD patterns of $Ni/Ce_{0.75}Zr_{0.25}O_{2-\delta}$ catalysts with the support obtained using the Pechini route. Both samples show the characteristic reflections corresponding to cubic fluorite-like structure and NiO.

The unit cell parameter a of impregnated $Ni/Ce_{0.75}Zr_{0.25}O_{2-\delta}$ ($Ni/CZ_{P\text{-}im}$) and one-pot sample ($Ni/CZ_{P\text{-}op}$) is equal to 5.357 Å and 5.358 Å, respectively, which coincides with the value for the initial $Ce_{0.75}Zr_{0.25}O_{2-\delta}$ support (5.357 Å). This fact implies that Ni is not incorporated into the fluorite lattice. According to the X-ray diffraction data, the average crystallite size of the fluorite-like phase did not depend on the preparation method and varied within 9–12 nm (Table 1). The NiO phase was detected for both samples, the size of its crystallites varied within the 18–25 nm range.

The Raman spectrum of $Ce_{0.75}Zr_{0.25}O_{2-\delta}$ samples prepared by both methods shows a strong peak at 470 cm^{-1}, corresponding to the main cubic fluorite phase (Figure 2b) [50]. This peak corresponds to the fundamental mode with F_{2g} symmetry, which can be assigned to a symmetric O–Ce–O stretching. In addition to the F_{2g} mode, the Raman spectra of impregnated samples show another strong band at 600 cm^{-1}, whereas for the one-pot sample, there is one more additional weak band at 232 cm^{-1}. These bands are related to the formation of lattice defects, mostly oxygen vacancies [51]. The intensity of defects induced bands I(D1 + D2) in the range 500–700 cm^{-1} was higher for samples with a larger defects concentration, therefore, the $\omega = I(D1 + D2)/I_{F2g}$ ratio, reported in Figure 1b in the frame, was used as a defect sensitive parameter [6,52,53]. In the case of $Ce_{0.75}Zr_{0.25}O_{2-\delta}$, regardless of the preparation method, oxygen defects concentration is low, defects can be related only to the difference of the ionic radii of Zr^{4+} and Ce^{4+}. For catalysts, the $I(D1 + D2)/I_{F2g}$ ratios are orders of magnitude larger than

those of supports. The appearance of a broad band at about 230 cm^{-1} was also revealed in the case of $Ni/CZ_{P\text{-}op}$ samples. The peak at 230 cm^{-1} corresponded to the second-order transverse acoustic mode of ceria, and that at 1180 cm^{-1} to the second-order longitudinal mode of ceria [53,54].

Figure 3a shows the XRD patterns of $Ni/Ce_{0.75}Zr_{0.25}O_{2-\delta}$ catalysts prepared using SCS. In distinction to other samples, the diffraction pattern of the CZsc sample synthesized in supercritical media without calcination shows only the broad reflections which were indexed within space group Fm3m as a cubic phase of the CeO_2–ZrO_2 solid solution (Figure 3a, Table 2). The Raman spectrum of this sample shows the presence of weak broad peaks of a low intensity at 450–700 cm^{-1}, also indicating that the crystal structure is not completely formed (Figure 3b).

Table 2. Physicochemical properties of supports and 5%Ni/Ce-Zr(Ti)O_2 catalysts.

Code	SSA, m^2/g	V_{total}, cm^3/g	T max of Peaks, °C/ H_2 Consumption, mmol $H_2 \times 10^{-6}$ g_{comp}^{-1}							
			T_1	T_2	T_3	T_4	T_5	T_6	T_7	Total
CZ_p	44	0.159	-	-	450/ 209	555/ 519	761/ 752	-	-	1484
$Ni/CZ_{P\text{-}im}$	35	0.143	240/ 143	308/ 401	449/ 757	511/ 199	765/ 660	-	-	2166
$Ni/CZ_{p\text{-}op}$	14	0.160	281/ 122	341/ 281	395/ 80	410/ 498	579/ 463	840/ 421	-	1873
CZ_{sc}	21	0.150	-	-	412/ 116	557/ 616	801/ 724	-	-	1344
$Ni/CZ_{sc\text{-}im}$	20	0.144	238/ 145	313/ 402	380/ 143	451/ 605	557/ 371	816/ 703	-	2192
$Ni/CZ_{sc\text{-}op}$	13	0.126	255/ 347	294/ 119	350/ 249	475/ 748	764/ 572	-	-	2016
$CT_{0.1}Z_{sc}$	34	0.165	-	-	491/ 256	575/ 338	769/ 581	-	-	1185
$Ni/CT_{0.1}Z_{sc\text{-}im}$	23	0.184	245/ 131	339/ 429	416/ 95	505/ 662	588/ 277	644/ 77	812/ 619	2306
$Ni/CT_{0.1}Z_{sc\text{-}op}$	16	0.143	257/ 262	319/ 108	340/ 314	413/ 328	532/ 762	725/ 613	-	2396
$Ni/CT_{0.2}Z_{sc\text{-}op}$	11	0.102	-	291/ 392	353/ 128	461/ 1153	587/ 384	756/ 641	-	2700

XRD patterns of 5% $Ni/Ce_{0.75}Zr_{0.25}O_{2-\delta}$ ($Ni/CZ_{sc\text{-}im}$) prepared by the impregnation of the support CZ_{sc} showed the presence of crystalline NiO, while for the 5% $Ni/Ce_{0.75}Zr_{0.25}O_{2-\delta}$ ($Ni/CZ_{sc\text{-}op}$) catalyst obtained by the one-pot route in supercritical conditions, crystalline NiO is practically not observed (Figure 3a). The presence of crystalline nickel oxide in the $Ni/CZ_{sc\text{-}im}$ indicates that the particles are not uniformly distributed over the surface, which leads to the formation of bulk crystalline structures. This phenomenon negatively affects the process of dry reforming of methane, since it catalyzes such reactions as the Boudouard reaction and the decomposition of methane [16,45]. The average crystallite size of NiO for $Ni/CZ_{sc\text{-}op}$ is reduced to 19.5 nm, compared to $Ni/CZ_{sc\text{-}im}$ (30 nm). According to the Raman data (Figure 3b) for all SCS samples, the presence of a single peak at 470 cm^{-1} confirms formation of the main crystal phase with cubic fluorite-like structure, which agrees with X-ray structural data. As in the case of Pechini samples, the Raman spectra of impregnated and one-pot samples have other strong bands at 500–600 cm^{-1}. The formation of the band at about 560 cm^{-1} (oxygen vacancies) is caused by various oxidation states of the introduced cation, while the band at about 600 cm^{-1} appears due to dissimilar ionic radius of the dopant compared to that of Ce^{4+} [52]. The parameter ω of catalysts in the case of samples obtained by the Pechini method were orders of magnitude larger than those of the support. In the case of the $Ni/CZ_{P\text{-}op}$ sample, its value is higher than that for the $Ni/CZ_{sc\text{-}im}$.

3.2. Structural Properties of Supports Doped by Ti and Catalysts Ni/$Ce_{0.75}Ti_xZr_{0.15-x}O_{2-\delta}$

The XRD patterns of all Ni/$Ce_{0.75}Ti_xZr_{0.15-x}O_{2-\delta}$ catalysts are mainly similar to the patterns of Ni/$Ce_{0.75}Zr_{0.25}O_{2-\delta}$ showing reflections of CeO_2–ZrO_2 complex oxides (Figure 4). After the introduction of titanium, the overall mixed oxide structure of the solid solution with the cubic lattice is retained. As also confirmed by Raman spectroscopy (Figure 4b), the incorporation of dopant Ti cations into the $Ce_{0.75}Zr_{0.25}O_{2-\delta}$ lattice occurs.

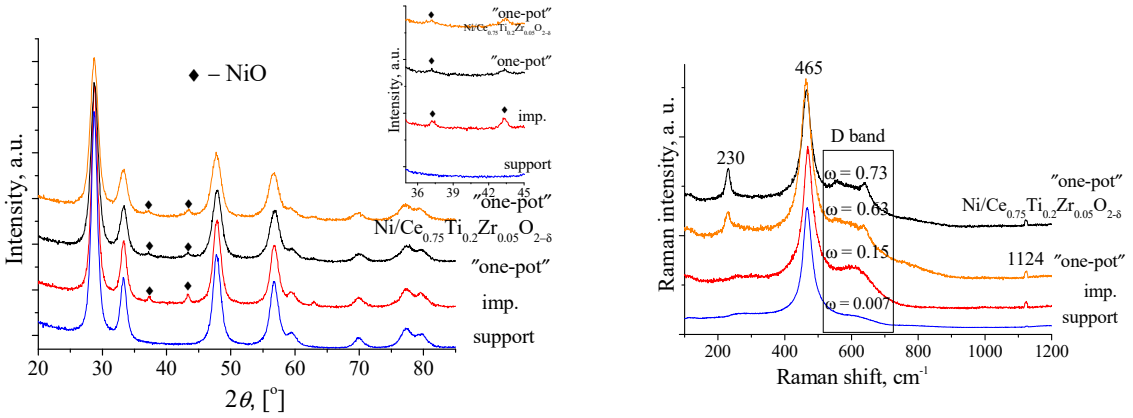

(**a**) (**b**)

Figure 4. XRD patterns (**a**) and Raman spectra (**b**) of Ni/$Ce_{0.75}Ti_{0.1}Zr_{0.15}O_{2-\delta}$ one-pot catalysts prepared in supercritical conditions and calcined at 700 °C.

In accordance with the Vegard law, by increasing the dopant (having a lower ionic radius) amount, a gradual decrease of the unit cell volume should be observed. This is evident when Zr is introduced into the CeO_2 lattice since there is a difference between the ionic radii of Ce^{4+} (0.97Å) and Zr^{4+} (0.84Å) [55]. The lattice constant of the initial CZ_{sc} support is 5.368 Å and this value is less than for CeO_2 (a = 5.411Å; PDF#340394). However, when $Ce_{0.75}Zr_{0.25}O_2$ Zr^{4+} cations were replaced by Ti^{4+}, the volume of the cubic unit cell increased. The unit cell parameter **a** of $Ce_{0.75}Ti_{0.1}Zr_{0.15}O_{2-\delta}$ is 5.378Å. With increasing the amount of titanium, the unit cell parameter is further increased and for $CT_{0.2}Z_{sc\text{-}op}$ a = 5.393 Å (Table 1). The question is why it happens, since the ionic radius of Ti^{4+} (the coordination number (c.n.) = 8) r = 0.74 Å and the ionic radius of Zr^{4+} (c.n. = 8) r = 0.84 Å.

This dependence can be clarified by the number of oxygen vacancies estimated using the Rietveld refinement. Figure 5 shows the dependence between the unit cell parameter and oxygen deficiency (δ) for initial supports, and it is clear that the parameter is increased with increase of the oxygen vacancies number. It is known that the formation of oxygen vacancies is associated with a partial reduction of Ce^{4+} to Ce^{3+} [56,57]. Since the radius of Ce^{3+} ions (1.14 Å) is greater than that of Ce^{4+} (0.97 Å), the appearance of a trivalent cation leads to an increase in the lattice constant. For a series of catalysts prepared using one-pot synthesis, an increase of the lattice parameter with an increasing titanium amount and number of oxygen vacancies is also observed. It could not be excluded that a part of the titanium cations can also be in 3+ state, thus having a higher cationic radius and increasing the lattice constant as well.

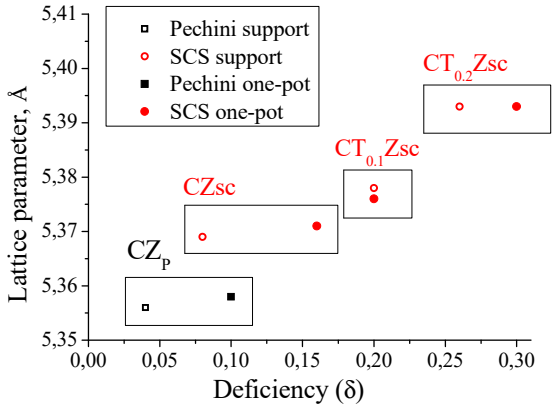

Figure 5. Dependence of the lattice parameter of initial supports and one-pot catalysts on the oxygen deficiency (δ).

As in the case of $Ce_{0.75}Zr_{0.25}O_{2-\delta}$, the oxygen defects concentration in $Ce_{0.75}Ti_{0.1}Zr_{0.15}O_{2-\delta}$ is low, so generation of defects can only be explained by the difference between the ionic radii of Ti^{4+} and Ce^{4+}. The $\omega = I(D1+D2)/I_{F2g}$ ratio of the intensities of induced bands I (D1 + D2) in the range 500–700 cm^{-1} is shown in Figure 4a. This ratio was higher for the catalysts with a larger defect concentration. Furthermore, just as in the case of samples $Ni/Ce_{0.75}Zr_{0.25}O_{2-\delta}$, the maximum value of this parameter is reached for the one-pot catalyst.

The XRD patterns of all catalysts are mainly similar. For one-pot catalysts, the broad reflections of NiO are observed. This is an indication of the high dispersion of nickel oxide phase achieved in these samples. The introduction of nickel does not have any noticeable effect on the particle size of supports (8.5–10 nm). The calculated NiO crystallite size for $Ni/CT_{0.1}Z_{sc\text{-}im}$ is found to be 20 nm, but it is decreased for the one-pot catalyst (13–15 nm).

3.3. Textural Characterization

The isotherms of nitrogen adsorption–desorption for the catalysts are shown in Figure 6a,b. The isotherms for the most samples correspond to the II type according to the IUPAC classification [58], which is characteristic for macroporous solids. Regardless of the preparation method of the catalysts, for samples prepared in supercritical alcohols multimodal pore size distribution is observed (Figure 6c,d). It depends on the support composition and includes micropores (d~4 nm) and macropores (50–200 nm). The introduction of titanium cations to $Ce_{0.75}Zr_{0.25}O_{2-\delta}$ led to an increase of pore size.

Only the $Ni/CZ_{P\text{-}im}$ isotherm fits to the IV type with H3 shaped hysteresis loop, characterizing the mesoporous structure. This type is observed for solids consisting of agglomerates of particles with nonuniform size and shape.

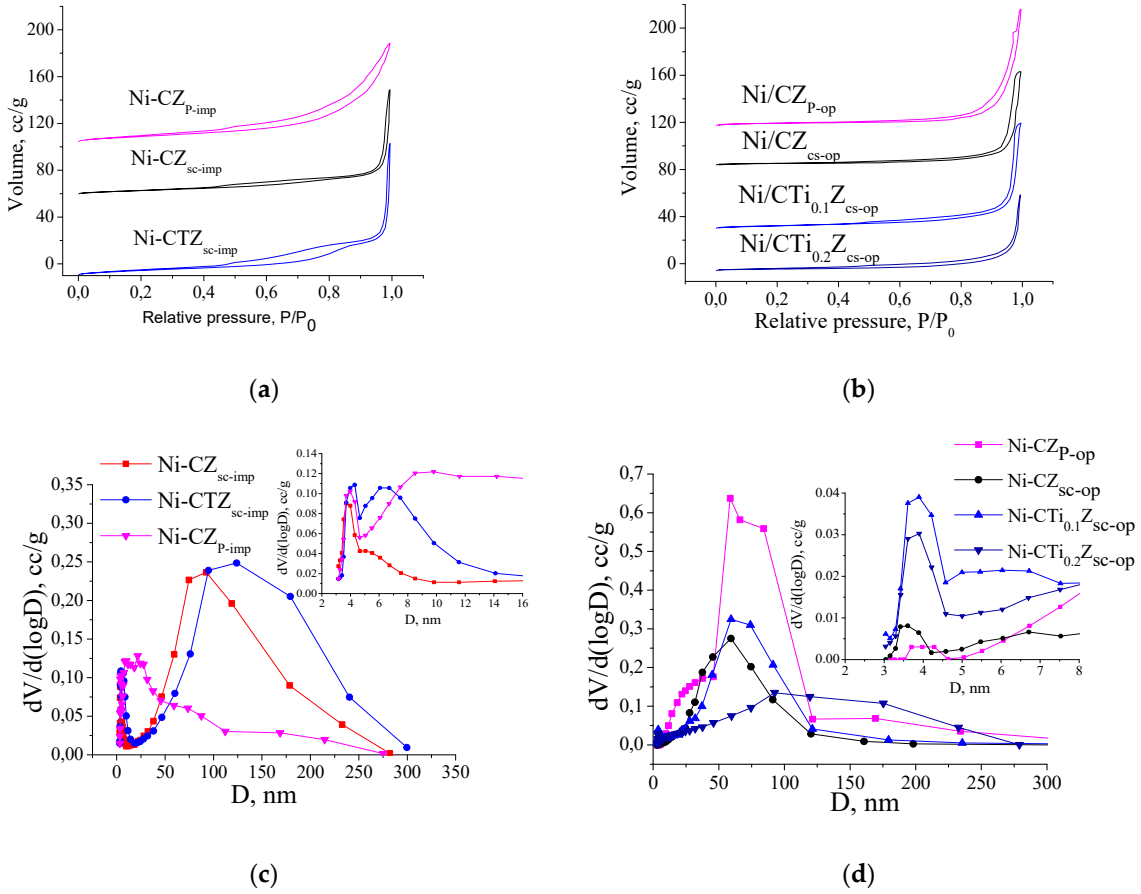

Figure 6. Adsorption–desorption isotherms and the pore size distribution of catalysts: (**a**,**c**) impregnated and (**b**,**d**) one-pot catalysts.

Table 2 shows the BET specific surface area (SSA) of fresh ceria–zirconia mixed oxides prepared using supercritical synthesis and the Pechini method and impregnated and one-pot catalysts. For SCS supports, the introduction of titanium cations into the Ce-Zr oxide structure leads to increase in the specific surface area. The addition of Ni results in decreasing SSA of all catalysts irrespective of the preparation method. For one-pot samples, this decrease may be caused by the influence of nickel cations on the formation of CeZrO framework during the synthesis and by the blocking a part of pores with NiO particles formed after calcination. So, in the case of catalysts obtained by impregnation, there is a slight decrease in the specific surface area due to the blocking of pores by NiO particles. Thus, the SSA of one-pot samples was lower than that of catalysts prepared by the traditional impregnation. However, preparation method (SCS or Pechini) almost has no additional influence on the value of their surface area.

3.4. H_2-TPR Characterization

H_2-TPR experiments for supports and Ni-containing catalysts were performed to investigate the redox characteristics; their results are presented in Figures 7 and 8 and in Table 2. Deconvolution of TPR curves into individual peaks and calculation of value of hydrogen consumption for each peak was carried out using the asymmetric Gauss decomposition method (AGDM). For all supports prepared using both synthesis methods, three peaks were observed after deconvolution, where the first two peaks (up to 550 °C) correspond to reduction of active surface oxygen, while the high-temperature hydrogen consumption is related to reduction of the bulk oxygen [13,59]. The introduction of titanium cations to $Ce_{0.75}Zr_{0.25}O_{2-\delta}$ led to the shift of the reduction peak toward higher temperatures, while the value of hydrogen consumption decreases as expected due to increase of the oxygen deficiency.

The Ce(Ti)ZrO_2 samples prepared by the supercritical synthesis did not show better reducibility compared to the Pechini ones.

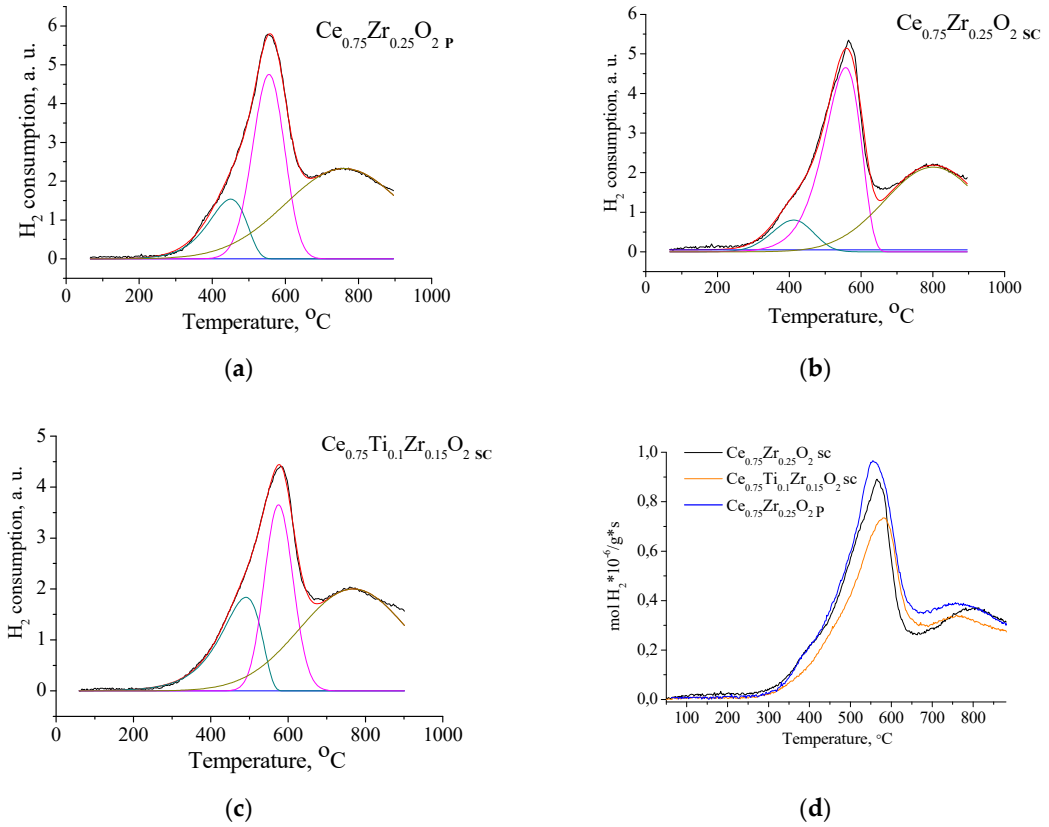

Figure 7. TPR-H_2 spectra of $Ce_{0.75}Zr_{0.75}O_{2-\delta}$ prepared by Pechini route (**a**) and in SC conditions (**b**), $Ce_{0.75}Ti_{0.1}Zr_{0.15}O_{2-\delta}$, prepared in supercritical alcohols (**c**); comparison of TPR-H_2 profiles of supports (**d**).

The H2-TPR spectra of Ni/Ce(Ti)ZrO_2 catalysts prepared by both methods are presented in Figure 8. It is a well-known fact that peaks in lower temperature regions are associated with the reduction of relatively free nickel oxide species, while peaks at higher temperatures indicate the reduction of complex NiO species, as a result of strong interaction with the support [60]. It is noticeable that the redox behavior of Ni particles is quite different depending on the method of metal introduction. The H_2-TPR curves for the impregnated catalysts are shifted to lower temperatures compared to the pure supports. Two main peaks were observed when $Ce_{0.75}Zr_{0.25}O_{2-\delta}$ oxides were used as supports. The first peak (311 °C) is related to the reduction of free NiO and the second higher intensity peak (455 °C) corresponds to NiO crystallites interacting with support. The profiles of the one-pot Ni/$Ce_{0.75}Zr_{0.25}O_{2-\delta}$ catalysts differ from that of impregnated samples. Thus, for the one-pot SC samples, the first clearly marked peak is shifted to lower temperature and new peak with the maxima at ~345–360 °C is observed. Shape of the TPR profiles for one-pot samples suggests existence of nickel oxide species with a wide range of particle sizes and interacting with support with different strength [51]. Hence, it could be concluded that the lattice oxygen in catalysts prepared using one-pot supercritical synthesis could migrate more easily than in the case of the Pechini method.

As shown in Figure 8, after the addition of Ti, the reduction peak is shifted toward higher temperatures, which implies a stronger interaction between NiO and the support. According to [1], the introduction of magnesium oxide shifted the reduction peak considerably towards higher temperatures as well. This obviously improved stability to nickel sintering and coking, and for the MgO-promoted Ni-$Ce_{0.8}Zr_{0.2}O_2$ catalyst, equilibrium conversions of methane and carbon dioxide were observed for 200 h without noticeable deactivation.

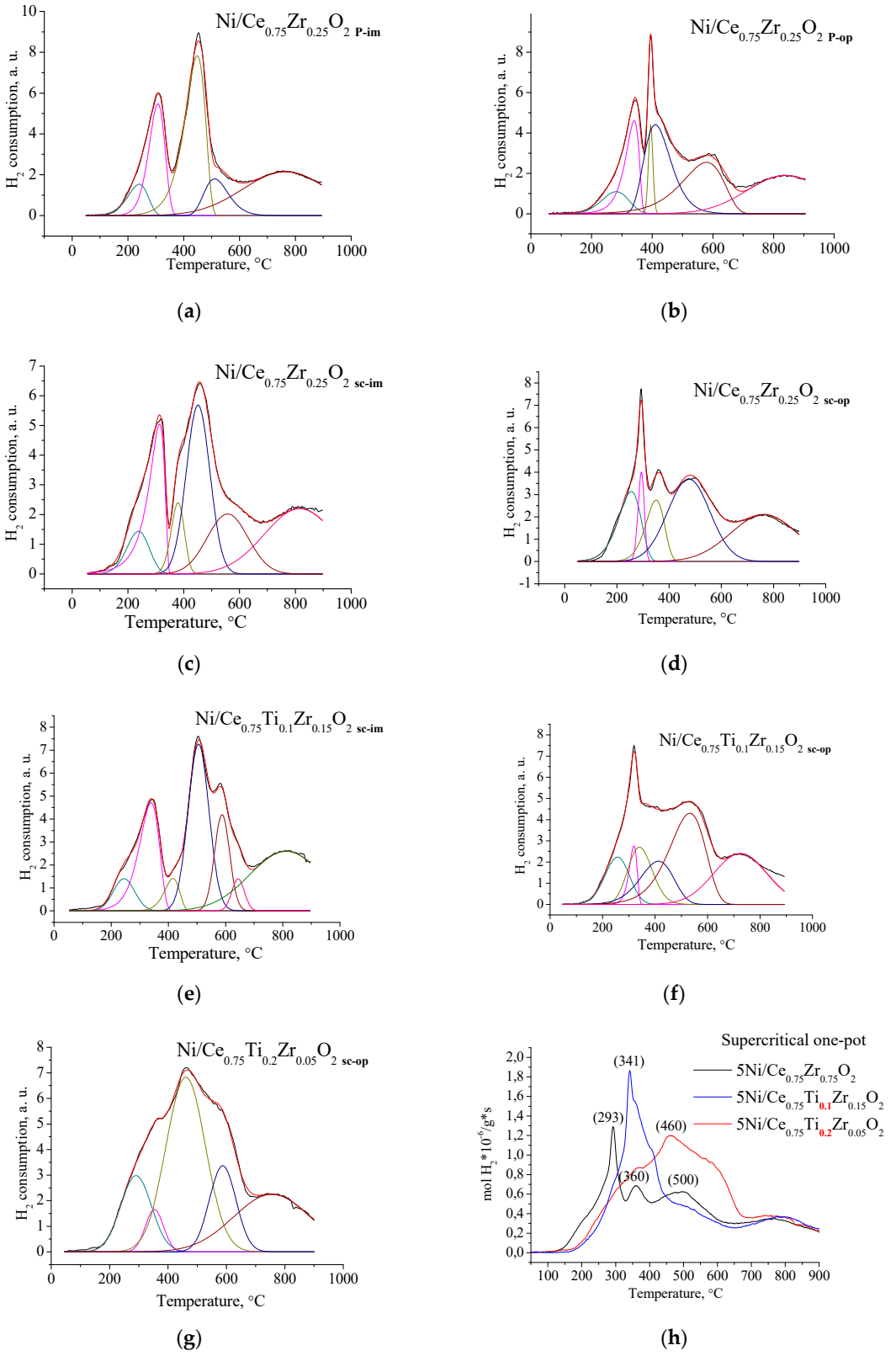

Figure 8. TPR-H_2 spectra of impregnated (**a**,**c**) and one-pot (**b**,**d**) 5%Ni/$Ce_{0.75}Zr_{0.75}O_{2-\delta}$ and impregnated (**e**) and one-pot (**f**,**g**) 5%Ni/$Ce_{0.75}Ti_xZr_{0.25-x}O_{2-\delta}$ prepared using the Pechini route and in SC conditions; comparison of TPR-H_2 profiles of one-pot catalyst of different compositions prepared in supercritical alcohols (**h**).

The values of the hydrogen consumption calculated for all deconvoluted peaks are presented in Table 2. The hydrogen consumption below 300 °C for the one-pot catalysts suggested more effective reduction of the surface oxygen, its amount being substantially larger than that for impregnated samples. The deconvoluted peaks of Ni/$CT_{0.1}Z_{sc\text{-}op}$ and Ni/$CT_{0.2}Z_{sc\text{-}op}$ corresponding to the main hydrogen consumption in the region of 300–800 °C are shifted to higher temperatures as compared with impregnated catalysts (Figure 8, Table 2). It can be explained by more difficult reduction of Ni^{2+} in the one-pot catalysts due to its stronger interaction with the support. According to XRD data, in one-pot samples, Ni is partially incorporated into ceria–zirconia solid solution [51], but is mainly present as NiO in the impregnated catalysts. The highest amount of removed oxygen, and, hence, the oxygen mobility was found for the Ni/$CT_{0.2}Z_{sc\text{-}op}$ sample (Table 2).

3.5. Morphology of Ceria–Zirconia Mixed Oxides

Particle morphology of the 5%Ni/$Ce_{0.75}Zr_{0.75}O_{2-\delta}$ and 5%Ni/$Ce_{0.75}Ti_xZr_{0.25-x}O_{2-\delta}$ samples was analyzed using a high-resolution TEM. Figure 9 shows TEM images of catalysts obtained using both preparation techniques and with both methods of Ni addition.

Ni/$CZ_{P\text{-}im}$

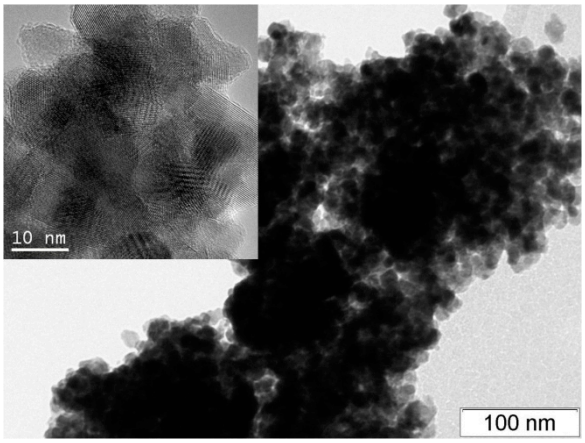

(**a**)

Ni/$CZ_{sc\text{-}im}$

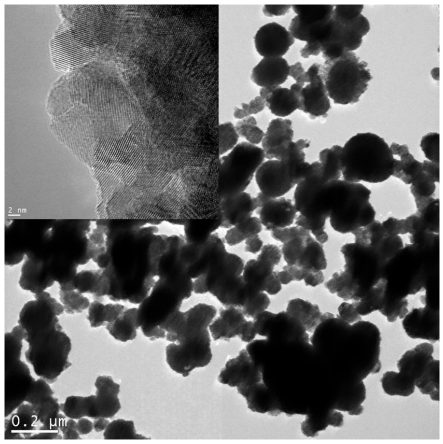

(**b**)

Ni/$CZ_{p\text{-}op}$

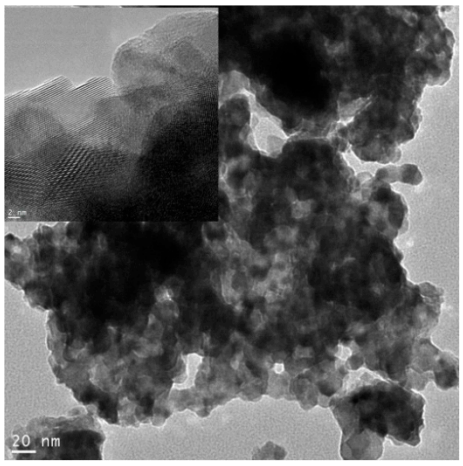

(**c**)

Ni/$CZ_{sc\text{-}op}$

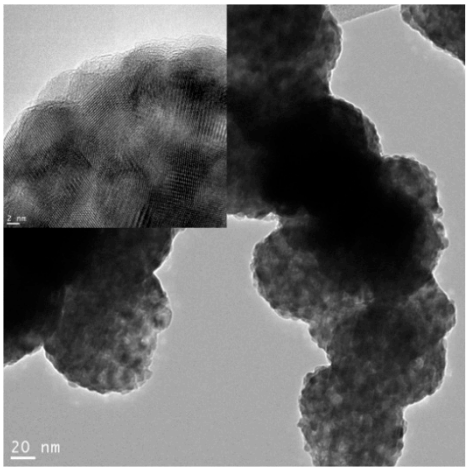

(**d**)

Figure 9. *Cont.*

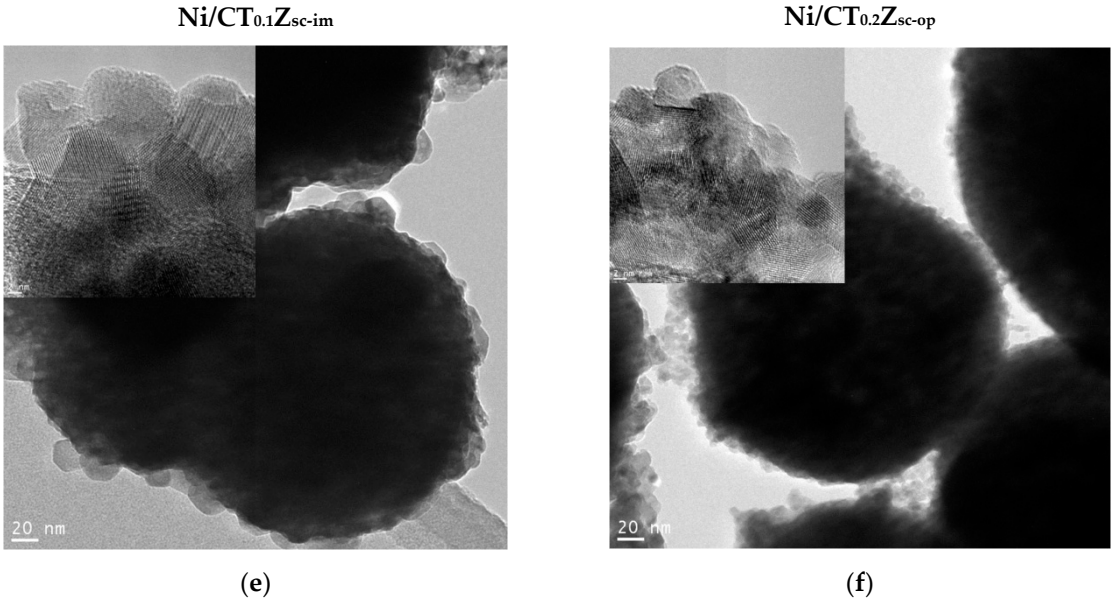

Figure 9. TEM images of impregnated (**a**,**b**) and one-pot (**c**,**d**) 5% Ni/$Ce_{0.75}Zr_{0.25}O_2$ prepared using the Pechini route (**a**,**c**) and supercritical synthesis (**b**,**d**) and Ti-doped catalysts (**e**,**f**) prepared in supercritical alcohols.

The average particle size of all samples is about 10–15 nm; that is consistent with XRD data. Particles of catalysts prepared by the Pechini method (Figure 9a,c) have a disordered shape and are assembled into chaotically formed agglomerates. Synthesis in supercritical alcohols results in formation of particles with a more spherical shape. They are packed into large spherical aggregates with diameter more than 100 nm. Formation of such aggregated CeO_2 and $Ce_{1-x}Zr_xO_2$ in bigger spherically-shaped nanostructured assemblies (20–100 nm in diameter) was shown in [61].

The addition of nickel at the stage of oxide preparation in the one-pot method, as well as doping with titanium, leads to formation of agglomerates with more ideal spherical morphology.

The images of HAADF-STEM with EDX analysis demonstrate distribution of elements in samples (Figure 10). Ce and Zr cations of the initial support, as well as Ti cations in doped supports, are uniformly distributed in the oxide structure of all samples, irrespective of the preparation method. The nickel distribution nature is more complex, partially depending on the method of preparation. For impregnated SCS samples, it can be assumed that addition of titanium to the support promotes a more uniform distribution of nickel after deposition (Figure 10 a,b).

Generally, it could be expected that addition of nickel during the oxide synthesis will contribute to its more homogeneous distribution. However, in the case of the Pechini method, this assumption turned out to be wrong and nickel is present as separate large particles (Figure 11a) (even at low nickel content in the investigated area), which is consistent with large NiO crystallite size estimated from XRD data. One-pot synthesis in supercritical alcohols allows one to obtain more uniform distribution of Ni species (Figure 11b), which confirms better mixing of components in these conditions.

Ni/CZ$_{sc\text{-}im}$

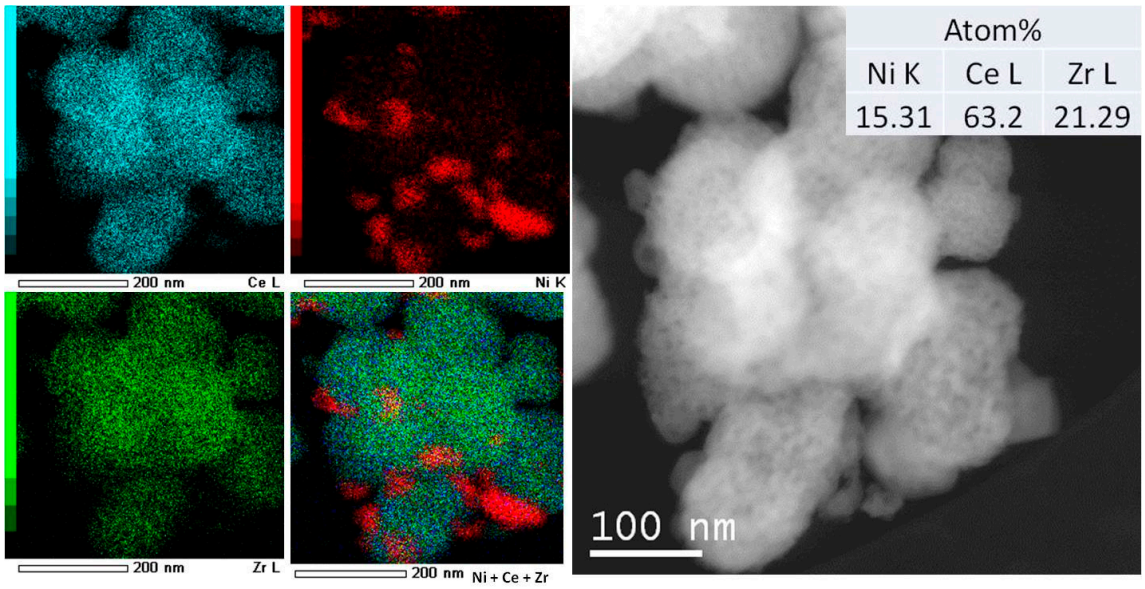

(**a**)

Ni/CT$_{0.1}$Z$_{sc\text{-}im}$

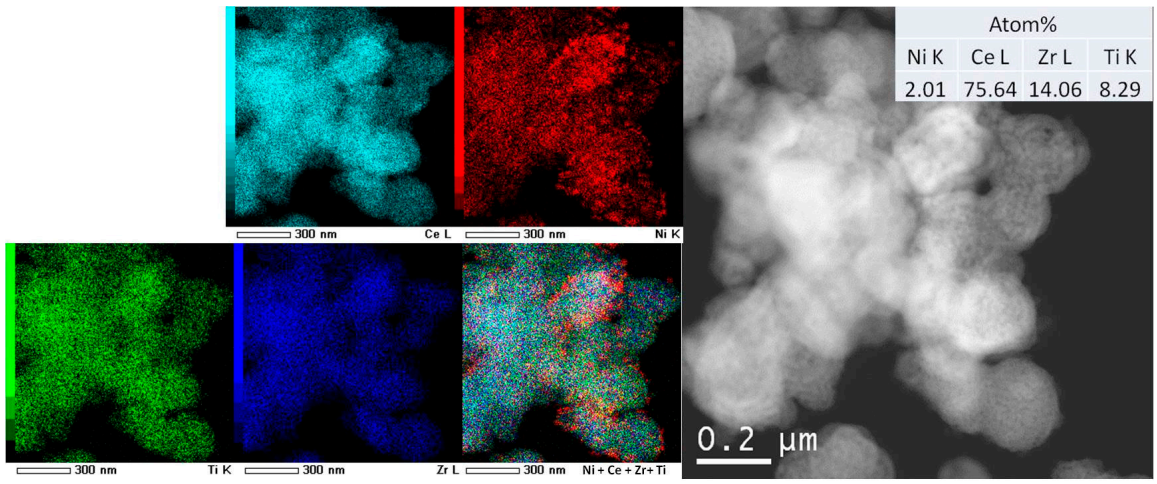

(**b**)

Figure 10. HAADF-STEM images with EDX analysis of the fresh impregnated 5% Ni/$Ce_{0.75}Zr_{0.25}O_2$ prepared using the Pechini route (**a**) and 5% Ni/$Ce_{0.75}Ti_{0.1}Zr_{0.15}O_{2-\delta}$ prepared using supercritical synthesis (**b**).

Ni/CZ$_{P\text{-}op}$

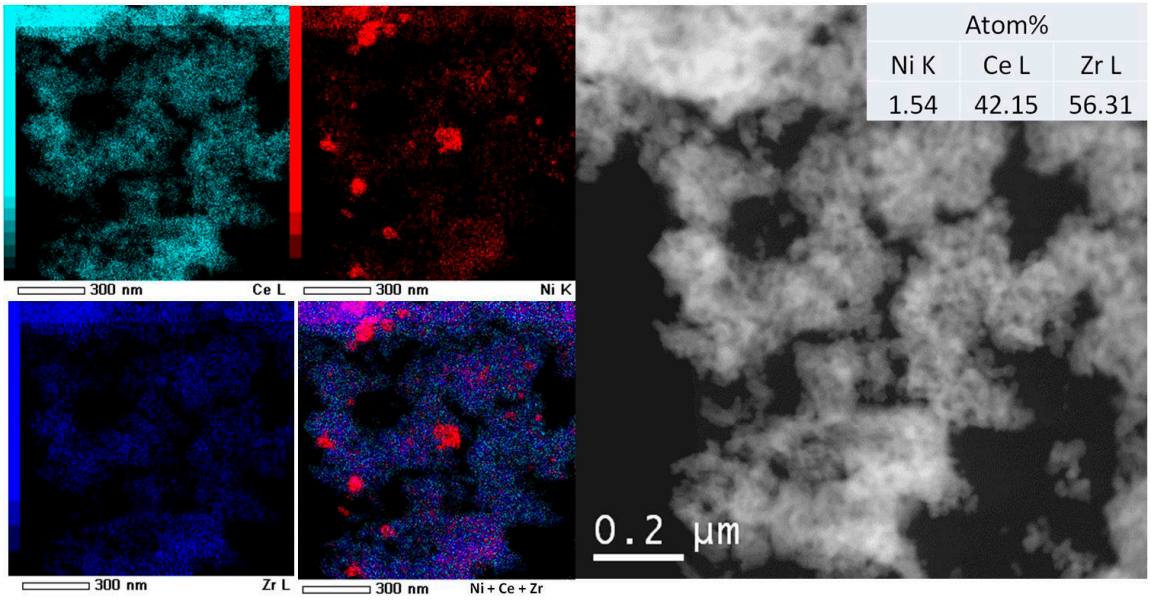

(**a**)

Ni/CT$_{0.2}$Z$_{sc\text{-}op}$

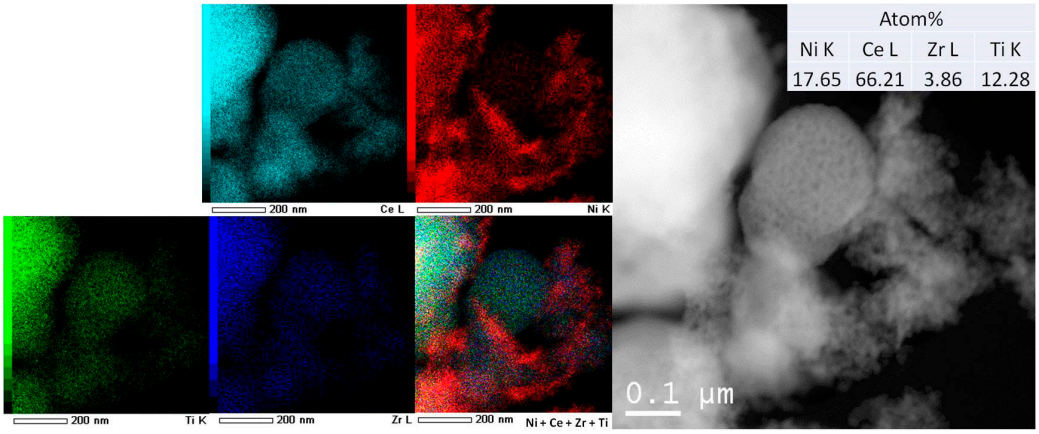

(**b**)

Figure 11. HAADF-STEM images with EDX analysis of the fresh one-pot 5% Ni/$Ce_{0.75}Zr_{0.25}O_2$ prepared using the Pechini route (**a**) and 5% Ni/$Ce_{0.75}Ti_{0.2}Zr_{0.05}O_{2-\delta}$ prepared using supercritical synthesis (**b**).

All catalysts after tests in methane dry reforming have also been investigated using TEM. Figure 12a,b demonstrates images of impregnated 5% Ni/$Ce_{0.75}Zr_{0.25}O_2$ catalysts. It can be seen that the surface of SCS sample is covered with carbon filaments, while Ni/$CZ_{P\text{-}im}$ is free from carbon, which could explain its higher activity. For the Ti-doped SCS catalyst, carbon filaments are also observed (not shown). During catalytic tests, nickel is segregated to the surface in the form of metal particles with sizes 10–20 nm. Some metal particles are breaking away from the oxide support during the growth of carbon fibers, which might lead to a drop in catalytic activity.

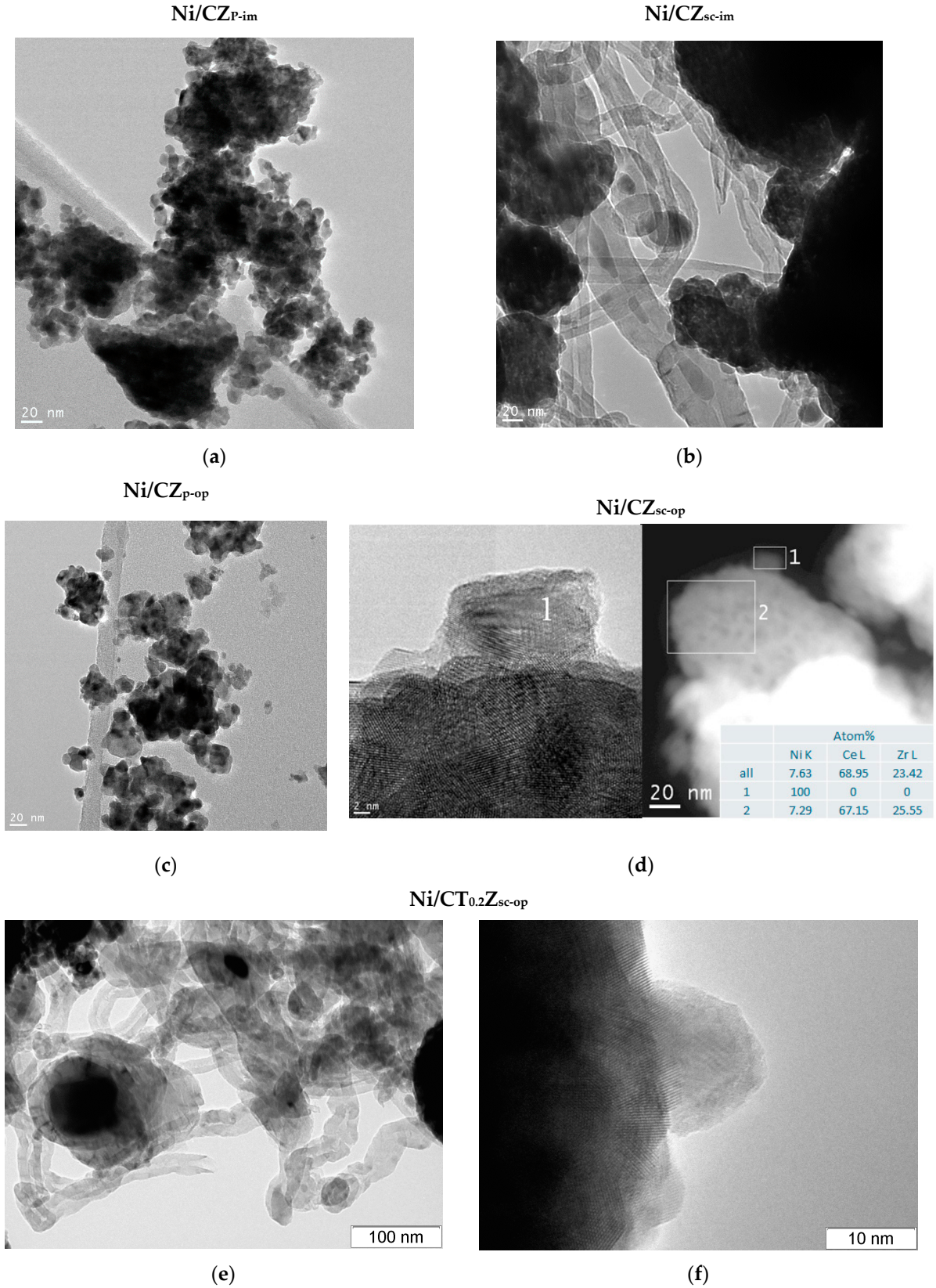

Figure 12. TEM images of impregnated (**a**,**b**) and one-pot (**c**,**d**) 5% $Ni/Ce_{0.75}Zr_{0.25}O_2$ catalysts prepared using the Pechini route (**a**,**c**) and supercritical synthesis (**b**,**d**) as well as Ti-doped one-pot catalyst (**e**,**f**) prepared in supercritical alcohols.

In the case of one-pot 5% Ni/$Ce_{0.75}Zr_{0.25}O_2$ catalysts, there are no coke depositions for both preparation methods (Figure 12c,d). It can be explained by a stronger interaction between the nickel particles and oxide support. Figure 11d demonstrates a nickel particle strongly interacting with support and covered by loose oxide layers, mainly containing nickel oxide, though traces of Ce and Zr cations could be present at the surface as well.

Carbon filaments are also observed over the surface of Ni/$CT_{0.2}Z_{sc\text{-}op}$ catalyst (Figure 12e), despite its high activity in DRM. However, there is not necessarily a relationship between carbon formation and activity decrease since this type of carbon does not block catalyst surface and, thus, does not inhibit catalytic activity [62].

3.6. Methane Dry Reforming Studies

The evolution over time of CH_4 and CO_2 conversions over impregnated catalysts at reaction temperatures 600–750 °C is presented in Figure 13. A summary of catalytic data is given in Table 3. For all the catalysts, conversion of reagents increases significantly with the temperature due to the endothermic nature of this reaction. The reagent conversions are higher over the impregnated catalyst 5%Ni/$Ce_{0.75}Zr_{0.25}O_2$ prepared using the Pechini method (Figure 13a,b) as compared with the sample prepared using supercritical synthesis. The Ni/$CZ_{sc\text{-}im}$ catalyst with support obtained under supercritical conditions is characterized by a sufficiently higher catalytic activity at 600–650 °C, but at higher temperatures, its catalytic activity is lower than that for Ni/$CZ_{p\text{-}im}$. However, for the one-pot sample prepared using the supercritical route, CH_4 and CO_2 conversions and product concentrations are somewhat higher than for the impregnated catalyst Ni/$CZ_{sc\text{-}im}$, while catalytic activity of the one-pot Pechini sample is much lower (Table 3, Figure 14c,d); that may be due to the low dispersion of nickel species.

Table 3. Conversion of CH_4 (X) and CO_2, selectivity (S), concentration of H_2 and CO and H_2/CO revealed during DRM (T = 700–750 °C; contact time 10 ms; feed composition—15 vol% CH_4 + 15 vol% CO_2 + N_2) over impregnated and one-pot catalysts 5 wt% Ni/CZ(T).

Code	T, °C	X(CH_4), %	X(CO_2), %	S(CO), %	Concentration CO, $*10^{-3}$ mol/L	S (H_2), %	Concentration H_2, $*10^{-3}$ mol/L	H_2/CO
Ni/$CZ_{p\text{-}im}$	700	33	40	73	3.9	56	2.3	0.59
	750	48	55	75	5.4	44	3.5	0.54
Ni/$CZ_{p\text{-}op}$	700	9	13	65	1.1	44	0.5	0.42
	750	16	23	69	2.1	62	1.1	0.46
Ni/$CZ_{sc\text{-}im}$	700	29	32	75	3.1	62	2.1	0.69
	750	39	42	76	4.2	65	3.0	0.71
Ni/$CZ_{sc\text{-}op}$	700	28	35	73	3.4	65	2.2	0.65
	750	42	47	73	4.6	65	3.2	0.68
Ni/$CT_{0.1}Z_{sc\text{-}im}$	700	23	23	75	1.6	32	1.0	0.65
	750	33	34	74	2.6	33	1.7	0.68
Ni/$CT_{0.1}Z_{sc\text{-}op}$	700	28	34	74	3.4	35	1.3	0.40
	750	39	45	75	4.5	37	2.0	0.44
Ni/$CT_{0.2}Z_{sc\text{-}op}$	700	36	43	76	4.2	48	2.5	0.58
	750	50	54	76	5.5	52	3.6	0.63

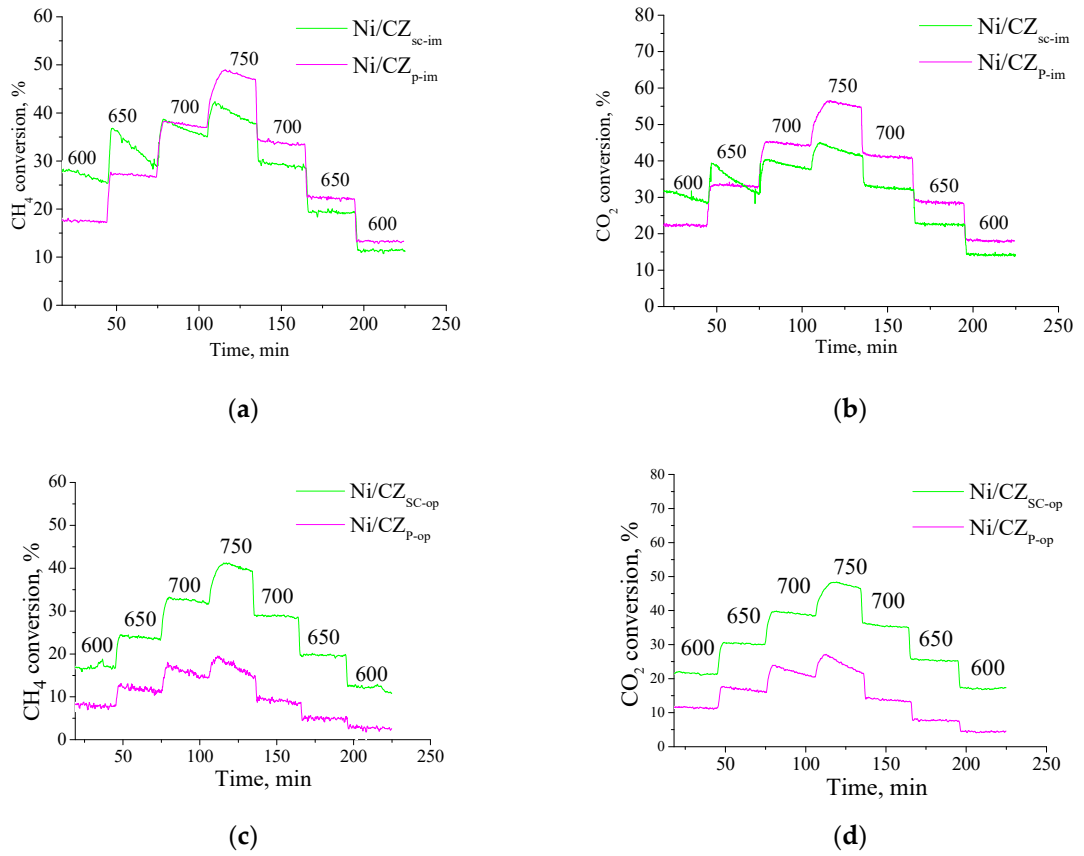

Figure 13. Methane and CO_2 conversions in thermal cycles 600–750–600 °C during dry reforming of CH_4 for impregnated (**a**,**b**) and one-pot (**c**,**d**) 5% Ni/$Ce_{0.75}Zr_{0.25}O_2$ catalysts prepared using the Pechini route and via supercritical synthesis.

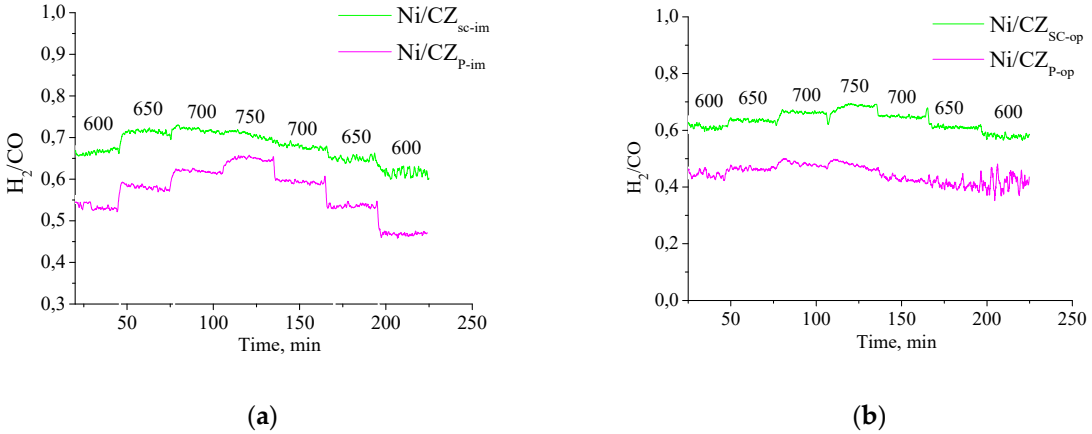

Figure 14. The dependence of H_2/CO ratio on reaction time for impregnated (**a**) and one-pot (**b**) 5% Ni/$Ce_{0.75}Zr_{0.25}O_2$ catalysts prepared using the Pechini route and via supercritical synthesis.

H_2/CO ratio for all catalysts is below 1 being in the range of 0.34–0.71 (Figure 14, Table 3). This fact is explained by the side competitive reaction of RWGS, which leads to an additional increase in the conversion of CO_2 compared to the CH_4 conversion and, as a result, to decrease of the content of hydrogen formed and a low H_2/CO ratio. With increasing temperature, there is a slight increase in the H_2/CO ratio for the Ni-CZsc-im sample, followed by a decrease at 700 °C and a drop in this ratio in the reverse cycle. In the temperature range of 700–750 °C, the H_2/CO ratio for the one-pot SCS sample was 0.65–0.68, which is comparable with the impregnated sample (0.69–0.71).

It was shown that introduction of 20 at% of Ti instead of Zr results in a significant improvement in DRM catalytic performance (Table 3). Short-term stability tests (Figure 15) reveal that methane conversion on a one-pot SCS ceria–zirconia sample doped by Ti immediately reaches maximum values at 750 °C and then gradually decreases during the experiment. An increase in the amount of introduced titanium leads to a noticeable increase in stability (Figure 16) as well. This fact apparently correlates with the highest oxygen mobility and storage capacity of $Ni/CT_{0.2}Z_{sc\text{-}op}$ catalyst revealed by H_2 TPR (Figure 8, Table 2), which helps to prevent coking. From the structural point of view, it is determined by the largest oxygen nonstoichiometry in heavily Ti-doped mixed ceria–zirconia oxide.

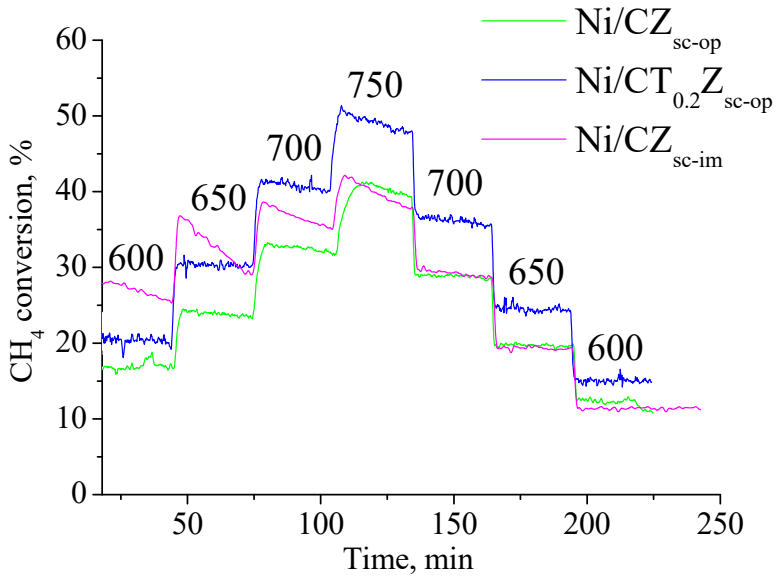

Figure 15. Comparison of effects of thermal cycling on CH_4 conversion in DRM over catalysts comprised of CZ and CTZ supports with Ni loaded by impregnation or one-pot methods.

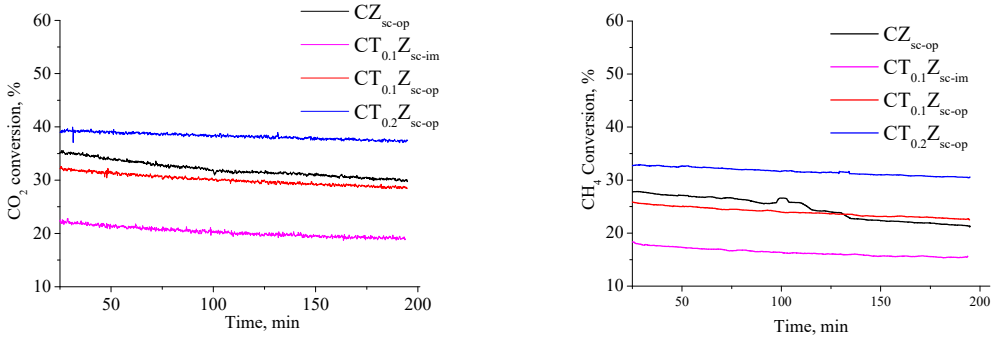

Figure 16. The dependence CO_2 (**a**) and CH_4 (**b**) on reaction time at 700 °C for the one-pot and impregnated SCS catalysts.

4. Conclusions

The mixed ceria–zirconia oxides also doped by Ti with cubic fluorite phase have been prepared using either the Pechini method or using continuous solvothermal flow synthesis in supercritical alcohols. For the first time using the supercritical synthesis method, a series of new one-pot $Ni/Ce(Ti)ZrO_2$ catalysts was prepared for the production of hydrogen and synthesis gas by means of methane dry reforming reaction. We compared catalysts prepared by two techniques: the standard incipient wetness impregnation and the one-pot synthesis. Catalysts prepared in supercritical isopropanol exhibited a higher catalytic activity and coking stability in CH_4 dry reforming reaction

than catalysts with a similar chemical composition prepared by the modified Pechini route. Based on the results of the catalytic tests, it was concluded that the highest conversion and maximum yield of products were achieved on the one-pot catalyst doped with titanium cations. The addition of Ni at the stage of oxide synthesis (so-called one-pot synthesis), according to TEM, resulted in a more uniform distribution of NiO particles on the surface of the catalyst, which confirms better mixing of components under these conditions. This uniform distribution of nickel provides a high activity and stability of one-pot catalysts. At the same time, after the reaction, the surfaces of many prepared catalysts are covered with carbon fibers, which, however, do not block the surface of the catalyst and do not lead to activity decrease.

Author Contributions: Methodology, M.S., Y.B., and E.S.; investigation, K.V., V.F., T.K., S.C., V.R., and A.I.; writing—Original draft preparation, Y.B. and E.S.; writing—Review and editing, V.S.; supervision, M.S.; project administration, M.S. All authors have read and agreed to the published version of the manuscript.

Funding: This research was funded by Russian Science Foundation, grant number 18-73-10167.

Conflicts of Interest: The authors declare no conflict of interest.

References

1. Jang, W.-J.; Shim, J.-O.; Kim, H.-M.; Yoo, S.-Y.; Roh, H.-S. A review on dry reforming of methane in aspect of catalytic properties. *Catal. Today* **2019**, *324*, 15–26. [CrossRef]
2. Usman, M.; Daud, W.W.; Abbas, H.F. Dry reforming of methane: Influence of process parameters—A review. *Renew. Sustain. Energy Rev.* **2015**, *45*, 710–744. [CrossRef]
3. Bradford, M.C.J.; Vannice, M.A. CO_2 Reforming of CH_4. *Catal. Rev.* **1999**, *41*, 1–42. [CrossRef]
4. Zhang, G.; Liu, J.; Xu, Y.; Sun, Y. A review of CH_4CO_2 reforming to synthesis gas over Ni-based catalysts in recent years (2010–2017). *Int. J. Hydrogen Energy* **2018**, *43*, 15030–15054. [CrossRef]
5. Wang, Y.; Yao, L.; Wang, S.; Mao, D.; Hu, C. Low-temperature catalytic CO_2 dry reforming of methane on Ni-based catalysts: A review. *Fuel Process. Technol.* **2018**, *169*, 199–206. [CrossRef]
6. Luisetto, I.; Tuti, S.; Romano, C.; Boaro, M.; Di Bartolomeo, E.; Kesavan, J.K.; Kumar, S.S.; Selvakumar, K. Dry reforming of methane over Ni supported on Odoped CeO_2: New insight on the role of dopants for CO_2 activation. *J. CO_2 Util.* **2019**, *30*, 63–78. [CrossRef]
7. Wolfbeisser, A.; Sophiphun, O.; Bernardi, J.; Wittayakun, J.; Föttinger, K.; Rupprechter, G. Methane dry reforming over ceria-zirconia supported Ni catalysts. *Catal. Today* **2016**, *277*, 234–245. [CrossRef]
8. Takano, A.; Tagawa, T.; Goto, S. Carbon Dioxide Reforming of Methane on Supported Nickel Catalysts. *J. Chem. Eng. Jpn.* **1994**, *27*, 727–731. [CrossRef]
9. Kambolis, A.; Matralis, H.; Trovarelli, A.; Papadopoulou, C. Ni/CeO_2-ZrO_2 catalysts for the dry reforming of methane. *Appl. Catal. A Gen.* **2010**, *377*, 16–26. [CrossRef]
10. Kim, S.S.; Lee, S.M.; Won, J.M.; Yang, H.J.; Hong, S.C. Effect of Ce/Ti ratio on the catalytic activity and stability of Ni/CeO_2-TiO_2 catalyst for dry reforming of methane. *Chem. Eng. J.* **2015**, *280*, 433–440. [CrossRef]
11. Swaan, H.; Kroll, V.; Martin, G.; Mirodatos, C. Deactivation of supported nickel catalysts during the reforming of methane by carbon dioxide. *Catal. Today* **1994**, *21*, 571–578. [CrossRef]
12. Kim, J.-H.; Suh, D.J.; Park, T.-J.; Kim, K.-L. Effect of metal particle size on coking during CO_2 reforming of CH_4 over Ni-alumina aerogel catalysts. *Appl. Catal. A Gen.* **2000**, *197*, 191–200. [CrossRef]
13. Trovarelli, A. *Catalysis by Ceria and Related Materials*, 2nd ed.; Università di Udine: Udine, Italy, 2002; Volume 2, p. 598.
14. Bonura, G.; Cannilla, C.; Frusteri, F. Ceria-gadolinia supported NiCu catalyst: A suitable system for dry reforming of biogas to feed a solid oxide fuel cell (SOFC). *Appl. Catal. B Environ.* **2012**, *121*, 135–147. [CrossRef]
15. Di Monte, R.; Kašpar, J. Nanostructured CeO_2-ZrO_2 mixed oxides. *J. Mater. Chem.* **2005**, *15*, 633–648. [CrossRef]
16. Kumar, P.; Sun, Y.; Idem, R.O. Comparative Study of Ni-based Mixed Oxide Catalyst for Carbon Dioxide Reforming of Methane. *Energy Fuels* **2008**, *22*, 3575–3582. [CrossRef]

17. Efstathiou, A.M.; Christou, S.Y.; Trovarelli, A.; Fornasiero, P. Investigation of the oxygen storage and release kinetics of model and commercial three-way catalytic materials by transient techniques. *Catal. Sci. Ser.* **2013**, *12*, 139–221.
18. Yang, Z.; Wei, Y.; Fu, Z.; Lu, Z.; Hermansson, K. Facilitated vacancy formation at Zr-doped ceria(111) surfaces. *Surf. Sci.* **2008**, *602*, 1199–1206. [CrossRef]
19. Mamontov, E.; Egami, T.; Brezny, R.; Koranne, M.; Tyagi, S. Lattice Defects and Oxygen Storage Capacity of Nanocrystalline Ceria and Ceria-Zirconia. *J. Phys. Chem. B* **2000**, *104*, 11110–11116. [CrossRef]
20. Fornasiero, P.; Dimonte, R.; Rao, G.; Kaspar, J.; Meriani, S.; Trovarelli, A.; Graziani, M. Rh-Loaded CeO_2-ZrO_2 Solid-Solutions as Highly Efficient Oxygen Exchangers: Dependence of the Reduction Behavior and the Oxygen Storage Capacity on the Structural-Properties. *J. Catal.* **1995**, *151*, 168–177. [CrossRef]
21. Zamar, F.; Trovarelli, A.; De Leitenburg, C.; Dolcetti, G. The direct room-temperature synthesis of CeO_2-based solid solutions: A novel route to catalysts with a high oxygen storage/transport capacity. *Stud. Surf. Sci. Catal.* **1996**, *101*, 1283–1292. [CrossRef]
22. Laosiripojana, N.; Assabumrungrat, S. Methane steam reforming over Ni/Ce-ZrO_2 catalyst: Influences of Ce-ZrO_2 support on reactivity, resistance toward carbon formation, and intrinsic reaction kinetics. *Appl. Catal. A Gen.* **2005**, *290*, 200–211. [CrossRef]
23. Khan, A.; Sukonket, T.; Saha, B.; Idem, R. Catalytic Activity of Various 5 wt % Ni/$Ce_{0.5}Zr_{0.33}M_{0.17}O_{2-\delta}$ Catalysts for the CO_2 Reforming of CH_4 in the Presence and Absence of Steam. *Energy Fuels* **2011**, *26*, 365–379. [CrossRef]
24. Dutta, G.; Waghmare, U.V.; Baidya, T.; Hegde, M.S.; Priolkar, K.R.; Sarode, P.R. Origin of Enhanced Reducibility/Oxygen Storage Capacity of $Ce_{1-x}Ti_xO_2$ Compared to CeO_2 or TiO_2. *Chem. Mater.* **2006**, *18*, 3249–3256. [CrossRef]
25. Luo, M.; Chen, J.; Chen, L.; Lu, J.; Feng, Z.; Li, C. Structure and Redox Properties of $Ce_xTi_{1-x}O_2$ Solid Solution. *Chem. Mater.* **2001**, *13*, 197–202. [CrossRef]
26. Lu, F.; Jiang, B.-B.; Wang, J.; Huang, Z.; Liao, Z.; Yang, Y.; Zheng, J. Promotional effect of Ti doping on the ketonization of acetic acid over a CeO_2 catalyst. *RSC Adv.* **2017**, *7*, 22017–22026. [CrossRef]
27. Yashima, M.; Morimoto, K.; Ishizawa, N.; Yoshimura, M. Zirconia-Ceria Solid Solution Synthesis and the Temperature-Time-Transformation Diagram for the 1:1 Composition. *J. Am. Ceram. Soc.* **1993**, *76*, 1745–1750. [CrossRef]
28. Mastelaro, V.R.; Briois, V.; De Souza, D.P.; Silva, C.L. Structural studies of a ZrO_2-CeO_2 doped system. *J. Eur. Ceram. Soc.* **2003**, *23*, 273–282. [CrossRef]
29. Li, G.; Wang, Q.; Zhao, B.; Shen, M.; Zhou, R. Effect of iron doping into CeO_2-ZrO_2 on the properties and catalytic behaviour of Pd-only three-way catalyst for automotive emission control. *J. Hazard. Mater.* **2011**, *186*, 911–920. [CrossRef]
30. Zhao, B.; Wang, Q.; Li, G.; Zhou, R. Effect of rare earth (La, Nd, Pr, Sm and Y) on the performance of Pd/$Ce_{0.67}Zr_{0.33}MO_{2-\delta}$ three-way catalysts. *J. Environ. Chem. Eng.* **2013**, *1*, 534–543. [CrossRef]
31. Le Gal, A.; Abanades, S.; Flamant, G. CO_2 and H_2O Splitting for Thermochemical Production of Solar Fuels Using Nonstoichiometric Ceria and Ceria/Zirconia Solid Solutions. *Energy Fuels* **2011**, *25*, 4836–4845. [CrossRef]
32. Fang, J.; Bao, H.; He, B.; Wang, F.; Si, D.; Jiang, Z.; Pan, Z.; Wei, S.; Huang, W. Interfacial and Surface Structures of CeO_2-TiO_2 Mixed Oxides. *J. Phys. Chem. C* **2007**, *111*, 19078–19085. [CrossRef]
33. Masui, T.; Fujiwara, K.; Peng, Y.; Sakata, T.; Machida, K.-I.; Mori, H.; Adachi, G.-Y. Characterization and catalytic properties of CeO_2-ZrO_2 ultrafine particles prepared by the microemulsion method. *J. Alloy. Compd.* **1998**, *269*, 116–122. [CrossRef]
34. Hadi, A.; Ismail, K.N.; Abu, M.N. Effect of Metals Oxides Loading on the Modification of Microstructure and Phase Transformation of Nanocrystalline $CeZrO_2$ Synthesized Using Water-in-oil-Microemulsion. *Procedia Soc. Behav. Sci.* **2015**, *195*, 2051–2060. [CrossRef]
35. Enzo, S.; Frattini, R.; Delogu, F.; Primavera, A.; Trovarelli, A. Neutron diffraction studies of ceria-zirconia catalysts prepared by high-energy mechanical milling. *Nanostruct. Mater.* **1999**, *12*, 673–676. [CrossRef]
36. Chen, Y.; Qi, M.; Yang, D.; Wu, K. Mechanical alloying of ceramics in zirconia-ceria system. *Mater. Sci. Eng. A* **1994**, *183*, L9–L12. [CrossRef]
37. Inagaki, M.; Kato, E. Hydrothermal Synthesis and Sintering of Fine Powders in CeO_2-ZrO_2 System. *J. Ceram. Soc. Jpn.* **1996**, *104*, 958–962. [CrossRef]

38. Sato, T.; Dosaka, K.; Yoshioka, T.; Okuwaki, A.; Torii, K.; Onodera, Y. Sintering of Ceria-Doped Tetragonal Zirconia Crystallized in Organic Solvents, Water, and Air. *J. Am. Ceram. Soc.* **1992**, *75*, 552–556. [CrossRef]
39. Tyrsted, C.; Becker, J.; Hald, P.; Bremholm, M.; Pedersen, J.S.; Chevallier, J.; Cerenius, Y.; Iversen, S.B.; Iversen, B.B. In-Situ Synchrotron Radiation Study of Formation and Growth of Crystalline $Ce_xZr_{1-x}O_2$ Nanoparticles Synthesized in Supercritical Water. *Chem. Mater.* **2010**, *22*, 1814–1820. [CrossRef]
40. Kim, J.-R.; Lee, K.-Y.; Suh, M.-J.; Ihm, S.-K. Ceria–zirconia mixed oxide prepared by continuous hydrothermal synthesis in supercritical water as catalyst support. *Catal. Today* **2012**, *185*, 25–34. [CrossRef]
41. Slostowski, C.; Marre, S.; Babot, O.; Toupance, T.; Aymonier, C. Near- and Supercritical Alcohols as Solvents and Surface Modifiers for the Continuous Synthesis of Cerium Oxide Nanoparticles. *Langmuir* **2012**, *28*, 16656–16663. [CrossRef] [PubMed]
42. Pradeep, E.K.; Habu, T.; Tooriyama, H.; Ohtani, M.; Kobiro, K. Ultra-simple synthetic approach to the fabrication of CeO_2-ZrO_2 mixed nanoparticles into homogeneous, domain, and core-Shell structures in mesoporous spherical morphologies using supercritical alcohols. *J. Supercrit. Fluids* **2015**, *97*, 217–223. [CrossRef]
43. Smirnova, M.Y.; Pavlova, S.N.; Krieger, T.A.; Bespalko, Y.N.; Anikeev, V.I.; Chesalov, Y.; Kaichev, V.; Mezentseva, N.V.; Sadykov, V. The Synthesis of $Ce_{1-x}Zr_xO_2$ Oxides in Supercritical Alcohols and Catalysts for Carbon Dioxide Reforming of Methane on Their Basis. *Russ. J. Phys. Chem. B* **2017**, *11*, 1312–1321. [CrossRef]
44. Adamski, A.; Legutko, P.; Dziadek, K.; Parkhomenko, K.; Aymonier, C.; Sadykov, V.A.; Roger, A.-C. Role of CeO_2-ZrO_2 Support for Structural, Textural and Functional Properties of Ni-based Catalysts Active in Dry Reforming of Methane. *E3S Web Conf.* **2019**, *108*, 02018. [CrossRef]
45. Sukonket, T.; Khan, A.; Saha, B.; Ibrahim, H.; Tantayanon, S.; Kumar, P.; Idem, R. Influence of the catalyst preparation method, surfactant amount and steam on CO_2 reforming of CH_4 over $5Ni/Ce_{0.6}Zr_{0.4}O_2$ Catalysts. *Energy Fuels* **2011**, *25*, 864–877. [CrossRef]
46. Roh, H.-S.; Potdar, H.; Jun, K.-W.; Kim, J.-W.; Oh, Y.-S. Carbon dioxide reforming of methane over Ni incorporated into Ce-ZrO_2 catalysts. *Appl. Catal. A Gen.* **2004**, *276*, 231–239. [CrossRef]
47. Marinho, A.L.; Rabelo-Neto, R.C.; Epron, F.; Bion, N.; Toniolo, F.S.; Noronha, F.B. Embedded Ni nanoparticles in $CeZrO_2$ as stable catalyst for dry reforming of methane. *Appl. Catal. B Environ.* **2020**, *268*, 118387. [CrossRef]
48. Gopalakrishnan, S.; Faga, M.G.; Miletto, I.; Coluccia, S.; Caputo, G.; Sau, S.; Giaconia, A.; Berlier, G. Unravelling the structure and reactivity of supported Ni particles in Ni-CeZrO2 catalysts. *Appl. Catal. B Environ.* **2013**, *138*, 353–361. [CrossRef]
49. Zagaynov, I.; Loktev, A.S.; Arashanova, A.; Ivanov, V.; Dedov, A.; Moiseev, I. Ni(Co)-$Gd_{0.1}Ti_{0.1}Zr_{0.1}Ce_{0.7}O_2$ mesoporous materials in partial oxidation and dry reforming of methane into synthesis gas. *Chem. Eng. J.* **2016**, *290*, 193–200. [CrossRef]
50. Escribano, V.S.; Lopez, E.F.; Panizza, M.; Resini, C.; Amores, J.M.G.; Busca, G. Characterization of cubic ceria–zirconia powders by X-ray diffraction and vibrational and electronic spectroscopy. *Solid State Sci.* **2003**, *5*, 1369–1376. [CrossRef]
51. Romero-Núñez, A.; Díaz, G. High oxygen storage capacity and enhanced catalytic performance of $NiO/Ni_xCe_{1-x}O_{2-\delta}$ nanorods: Synergy between Ni-doping and 1D morphology. *RSC Adv.* **2015**, *5*, 54571–54579. [CrossRef]
52. Li, L.; Chen, F.; Lu, J.-Q.; Luo, M.-F. Study of Defect Sites in $Ce_{1-x}M_xO_{2-\delta}$ (x = 0.2) Solid Solutions Using Raman Spectroscopy. *J. Phys. Chem. A* **2011**, *115*, 7972–7977. [CrossRef] [PubMed]
53. Deng, J.; Chu, W.; Wang, B.; Yang, W.; Zhao, X.S. Mesoporous $Ni/Ce_{1-x}Ni_xO_{2-y}$ heterostructure as an efficient catalyst for converting greenhouse gas to H_2 and syngas. *Catal. Sci. Technol.* **2016**, *6*, 851–862. [CrossRef]
54. Pu, Z.-Y.; Lu, J.-Q.; Luo, M.-F.; Xie, Y.-L. Study of Oxygen Vacancies in $Ce_{0.9}Pr_{0.1}O_{2-\delta}$ Solid Solution by in Situ X-ray Diffraction and in Situ Raman Spectroscopy. *J. Phys. Chem. C* **2007**, *111*, 18695–18702. [CrossRef]
55. Shannon, R.D. Revised effective ionic radii and systematic studies of interatomic distances in halides and chalcogenides. *Acta Crystallogr. Sect. A* **1976**, *32*, 751–767. [CrossRef]
56. Choudhury, B.; Choudhury, A. Ce^{3+} and oxygen vacancy mediated tuning of structural and optical properties of CeO_2 nanoparticles. *Mater. Chem. Phys.* **2012**, *131*, 666–671. [CrossRef]
57. Zhang, Z.; Han, N.; Wei, S.; Zhang, Y. Determination of active site densities and mechanisms for soot combustion with O_2 on Fe-doped CeO_2 mixed oxides. *J. Catal.* **2010**, *276*, 16–23. [CrossRef]

58. Leofanti, G.; Padovan, M.; Tozzola, G.; Venturelli, B. Surface area and pore texture of catalysts. *Catal. Today* **1998**, *41*, 207–219. [CrossRef]
59. Kim, J.-R.; Myeong, W.-J.; Ihm, S.-K. Characteristics in oxygen storage capacity of ceria-zirconia mixed oxides prepared by continuous hydrothermal synthesis in supercritical water. *Appl. Catal. B Environ.* **2007**, *71*, 57–63. [CrossRef]
60. Roh, H.-S.; Koo, K.Y.; Yoon, W.L. Combined reforming of methane over co-precipitated Ni-CeO_2, Ni-ZrO_2 and Ni-$Ce_{0.8}Zr_{0.2}O_2$ catalysts to produce synthesis gas for gas to liquid (GTL) process. *Catal. Today* **2009**, *146*, 71–75. [CrossRef]
61. Slostowski, C.; Marre, S.; Babot, O.; Toupance, T.; Aymonier, C. Effect of Thermal Treatment on the Textural Properties of CeO_2 Powders Synthesized in Near- and Supercritical Alcohols. *ChemPhysChem* **2015**, *16*, 3493–3499. [CrossRef]
62. Alberton, A.L.; Souza, M.M.V.M.; Schmal, M. Carbon formation and its influence on ethanol steam reforming over Ni/Al_2O_3 catalysts. *Catal. Today* **2007**, *123*, 257–264. [CrossRef]